18. Li S, Bhatt R, Megyesi J *et al.* PPAR-alpha ligand ameliorates acute renal failure by reducing CP-induced increased expression of renal endonuclease G. *Am J Physiol Renal Physiol* 2004; **287**: F990–F998.
19. Li S, Gokden N, Okusa MD *et al.* Anti-inflammatory effect of fibrate protects from CP-induced ARF. *Am J Physiol Renal Physiol* 2005; **289**: F469–F480.
20. Nagothu KK, Bhatt R, Kaushal GP *et al.* Fibrate prevents CP-induced proximal tubule cell death. *Kidney Int* 2005; **68**: 2680–2693.
21. Schonefeld M, Noble S, Bertorello AM *et al.* Hypoxia-induced amphiphiles inhibit renal NaK-ATPase. *Kidney Int* 1996; **49**: 1289–1296.
22. Feldkamp T, Kribben A, Roeser NF *et al.* Accumulation of nonesterified fatty acids causes the sustained energetic deficit in kidney proximal tubules after hypoxia–reoxygenation. *Am J Physiol Renal Physiol* 2005; **290**: F465–F477.
23. Portilla D, Li S, Nagothu KK *et al.* Metabolomic study of CP-induced nephrotoxicity. *Kidney Int* 2006; **69**: 2194–2204.
24. Colton HM, Falls JG, Ni H *et al.* Visualization and quantitation of peroxisomes using fluorescent nanocrystals: treatment of rats and monkeys with fibrates and detection in the liver. *Toxicol Sci* 2004; **80**: 183–192.
25. Kamijo A, Sugaya T, Hikawa A *et al.* Urinary excretion of fatty acid-binding protein reflects stress overload on the proximal tubules. *Am J Pathol* 2004; **165**: 1243–1255.
26. Gulati S, Singh AK, Irazu C *et al.* Ischemia-reperfusion injury: biochemical alterations in peroxisomes of rat kidney. *Arch Biochem Biophys* 1992; **295**: 90–100.
27. Klionsky DJ. The molecular machinery of autophagy: unanswered questions. *J Cell Sci* 2005; **118**: 7–18.
28. Cuervo AM. Autophagy in neurons: it is not all about food. *Trends Mol Med* 2006; **12**: 461–464.
29. Dunn WA, Cregg JM, Kiel J AKW *et al.* Pexophagy. The selective autophagy of peroxisomes. *Autophagy* 2005; **1**: 75–83.
30. Berkenstam A, Ahlberg J, Glaumann H. Isolation and characterization of autophagic vacuoles from rat kidney cortex. *Virchows Arch B Cell Pathol Incl Mol Pathol* 1983; **44**: 275–286.
31. Schrader M, Fahimi HD. Peroxisomes and oxidative stress. *Biochimica et Biophysica Acta* 2006; **1763**: 1755–1766.
32. Wanders RJ, Waterham HR. Biochemistry of mammalian peroxisomes revisited. *Annu Rev Biochem* 2006; **75**: 295–332.
33. Rottensteiner H, Theodoulou FL. The ins and outs of peroxisomes: coordination of membrane transport and peroxisomal metabolism. *Biochimica et Biophysica Acta* 2006; **1763**: 1527–1540.
34. Visser WF, van Roermund CWT, Ijlst L *et al.* Metabolite transport across the peroxisomal membrane. *Biochem J* 2007; **401**: 365–375.
35. Wanders RJ, van Roermund CW, Visser WF *et al.* Peroxisomal fatty acid α and β-oxidation in health and disease: new insights. *Adv Exp Med Biol* 2003; **544**: 293–302.
36. Ockner RK, Manning JA, Poppenhausen RB *et al.* A binding protein for fatty acids in cytosol of intestinal mucosa, liver, myocardium, and other tissues. *Science* 1972; **177**: 56–58.
37. Maatman RG, van den Westerlo EM, van Kuppevelt TH *et al.* Molecular identification of the liver and the heart-type fatty acid binding proteins in human and rat kidney. Use of the reverse transcriptase polymerase chain reaction. *Biochem J* 1992; **15**: 285–290.
38. Vancura A, Haldar D. Regulation of mitochondrial and microsomal phospholipid synthesis by liver fatty acid binding protein. *J Biol Chem* 1992; **267**: 14353–14359.
39. Raza H, Pongubala JR, Sorof S. Specific high affinity binding of lipooxygenase metabolites of arachidonic acid by liver fatty acid-binding protein. *Biochem Biophys Res Commun* 1989; **161**: 448–455.
40. Takikawa H, Kaplowitz N. Binding of bile acids, oleic acid, and organic anions by rat and human hepatic Z protein. *Arch Biochem Biophys* 1986; **251**: 385–392.
41. Faber K, Hvidberg V, Moestrup SK *et al.* Megalin is a receptor for apolipoprotein M, and kidney-specific megalin-deficiency confers urinary excretion of apolipoprotein M. *Mol Endocrinol* 2006; **20**: 212–218.
42. Masson P, Ohlsson P, Bjorkhem I. Combined enzymic-Jaffe method for determination of creatinine in serum. *Clin Chem* 1981; **27**: 18–21.
43. Kamijo A, Kimura K, Sugaya T *et al.* Urinary fatty acid-binding protein as a new clinical marker of the progression of chronic renal disease. *J Lab Clin Med* 2004; **143**: 23–30.
44. Kamijo-Ikemori A, Sugaya T, Obama A *et al.* Liver-type fatty acid-binding protein attenuates renal injury induced by unilateral ureteral obstruction. *Am J Pathol* 2006; **169**: 1107–1117.

Original Paper

nephron
Experimental
Nephrology

Nephron Exp Nephrol 2008;108:e19–e26
DOI: 10.1159/000112912

Received: July 11, 2007
Accepted: October 24, 2007
Published online: January 8, 2008

Urinary Human L-FABP Is a Potential Biomarker to Predict COX-Inhibitor-Induced Renal Injury

Tamami Tanaka[a] Eisei Noiri[a, d] Tokunori Yamamoto[b] Takeshi Sugaya[c]
Kousuke Negishi[a] Rui Maeda[d] Kazuo Nakamura[c] Didier Portilla[e]
Momokazu Goto[b] Toshiro Fujita[a]

[a]Departments of Nephrology and Endocrinology and Hemodialysis and Apheresis, Tokyo University Hospital, Tokyo, [b]Department of Urology, Nagoya University Hospital, Nagoya, [c]CMIC Co. Ltd., Tokyo, and [d]Center for NanoBio Integration, University of Tokyo, Tokyo, Japan; [e]Division of Nephrology, Department of Internal Medicine, University of Arkansas for Medical Sciences and Central Veteran Healthcare System, Little Rock, Ark., USA

Key Words
Biomarker development · Chronic renal injury · Cyclooxygenase inhibitors · L-type fatty acid binding protein

Abstract
Background/Aim: A strong demand exists for the development of sensitive biomarkers in the nephrology field. We propose urinary human L-type fatty acid binding protein (L-FABP) as an earlier biomarker to detect the outcome of chronic renal injury induced by cyclooxygenase (COX) inhibitors using human L-FABP transgenic mice. ***Methods:*** After consuming a low-sodium diet for 2 weeks, transgenic mice were administered meloxicam or celecoxib with the low-sodium diet. Mice were sacrificed 2 days and 4 weeks after starting COX inhibitors, and urine was collected 24 and 48 h and 1, 2, 3, and 4 weeks after starting COX inhibitors. Celecoxib-treated mice were divided into responders or nonresponders according to urinary L-FABP levels, and histology, urinary L-FABP and peritubular capillary blood flow were evaluated. ***Results:*** Meloxicam-treated mice showed a higher blood pressure than control mice. Urinary L-FABP was significantly increased in COX inhibitor-treated mice. Peritubular capillary blood flow in all meloxicam-treated mice and in some celecoxib-treated mice was significantly decreased. Although blood urea nitrogen was not increased, interstitial fibrosis and macrophage infiltration were revealed, especially in meloxicam-treated mice. Responders showed an increase of fibrotic areas and correlations between urinary L-FABP and peritubular capillary blood flow. ***Conclusion:*** Urinary L-FABP is capable of revealing chronic renal injury induced by COX inhibitors.

Introduction

The increasing population of geriatric individuals dictates that nonsteroidal anti-inflammatory drugs (NSAIDs) and cyclooxygenase (COX)-2 inhibitors must be prescribed more carefully because the renin-angiotensin-aldosterone system is more upregulated among older people than among younger people. Older people are often advised to reduce their sodium consumption when suffering from hypertension, diabetes mellitus, and chronic kidney disease [1, 2]. A low-sodium diet might further increase renin-angiotensin-aldosterone system activity. Moreover, the necessity of pain relief prescription medication will increase because of age-related low-

KARGER
Fax +41 61 306 12 34
E-Mail karger@karger.ch
www.karger.com

1660–2129/08/1081–0019$24.50/0

Accessible online at:
www.karger.com/nee

Eisei Noiri, MD, PhD
107 Lab., Departments of Nephrology and Endocrinology
University of Tokyo, 7-3-1 Hongo, Bunkyo
Tokyo 113-8655 (Japan)
Tel./Fax +81 3 5814 8696, E-Mail noiri-tky@umin.ac.jp

er back pain, osteoarthritis, and other causes. Most NSAIDs inhibit both COX-1 and COX-2 [3]. Selective inhibition of COX-2 is considered to be associated with most beneficial therapeutic anti-inflammatory efficacy in NSAIDs [4, 5]. Therefore, COX-2-selective inhibitors like meloxicam and a COX-2-specific inhibitor like celecoxib have been developed by pharmaceutical companies. In fact, COX-1 is constitutively expressed throughout the human body, playing crucial roles in normal gastrointestinal mucosa and platelet function. Inhibition of COX-1 is associated with nonbeneficial outcomes like gastrointestinal ulceration and only partial therapeutic efficacy because of bleeding tendencies induced by platelet dysfunction [6]. In the presence of inflammatory processes by endotoxins and cytokines, etc., COX-2 is an inducible enzyme. In the kidney, COX-2 is apparently expressed in a constitutive fashion; Cheng et al. [7] reported that the renal isoenzyme of COX-2 is capable of inhibiting renin secretion in macula densa [7] and that this decrease in renin secretion might consequently increase blood pressure and serum potassium levels and lead to edema formation and decreased glomerular filtration [8]. Therefore, the long-term aspects of the safety of COX-2 inhibitors are not yet fully understood because the exposure periods of those drugs are rather short, and inhibitors might be nephrotoxic. However, it is considerably difficult to monitor chronic nephrotoxicity and will be extremely difficult to anticipate it at an earlier time point after starting such prescriptions. This study investigates the applicability of urinary L-type fatty acid binding protein (L-FABP) to indicate potential renal damage. The dosage of the COX-2 inhibitors used for this study was nontoxic in rodents, but demonstrated different histological responses such as interstitial fibrosis after administration for 4 weeks. These effects were not detectable by a serum marker, blood urea nitrogen, but urinary L-FABP could differentiate between responders and nonresponders. Urinary L-FABP is a potential biomarker to monitor the occurrence of drug-induced nephrotoxicity during chronic treatment.

Materials and Methods

Materials

All chemical compounds were purchased from Wako Pure Chemical Industries (Osaka, Japan) unless otherwise specified. Celecoxib was provided by Pfizer (New York, N.Y., USA). Meloxicam was generously provided by Daiichi-Sankyo (Tokyo, Japan). Rat anti-mouse F4/80 macrophage antigen antibody (MCA497R) was purchased from Serotec (Raleigh, N.C., USA). All experiments were conducted in accordance with the NIH Guide for the Care and Use of Laboratory Animals [US Department of Health and Human Services, National Institutes of Health, NIH Publication No. 86-23, 1985]. The experimental protocol was qualified and approved by the Committee of Animal Resources of the University of Tokyo (No. 460).

Experimental Protocol

Before starting drug administration, the mice were fed a low-sodium diet (0.01% Na^+; Oriental Yeast, Tokyo) with water ad libitum for more than 2 weeks. This feeding pattern was continued after starting drug administration. The control group was fed a normal diet. Either meloxicam 2.5 mg/kg or celecoxib 20 mg/kg was dissolved in 0.5% carboxymethylcellulose and administered daily per os. The dosages used for both compounds were in the nontoxic range for mice based on previously published reports [9].

Measurement of Blood Pressure

The blood pressure was measured by tail cuff sensor (MK-2000; Muromachi Kikai, Tokyo) 2 weeks after feeding the low-sodium diet and 2 days and 4 weeks after starting meloxicam. The blood pressure was measured three times in each animal and averaged; the values were further averaged in each group.

Intravital CCD Video Analysis of the Peritubular Capillary Blood Flow

Renal cortical peritubular capillaries were measured 2 weeks after starting the low-sodium diet and 2 days after starting COX inhibitors. The renal cortical peritubular capillaries were viewed using a pencil-lens probe charge-coupled device video microscope with a 1-mm (diameter) tip, as previously described [10, 11]. The probe had a magnification of ×520, a depth of field <60 μm, and spatial resolution of 0.86 μm, permitting identification of individual erythrocytes. The probe was equipped with optical fibers transmitting light from a xenon AC 100-volt light source. Video signals were digitized using an analog-to-digital converter and recorded using a digital videocassette recorder (DVCAM; Sony, Tokyo) interfaced to a computer. The device (Scalar, Tokyo) used in this study was described previously [10]. The peritubular capillary blood flow was recorded by means of a pencil-lens microscope connected directly to the decapsulated renal surface. Images were recorded on digital videocassette tapes at a rate of 30 frames/s from the kidney. Animal cohorts are detailed in the Results section. Visualization of the images was improved on freeze frames using NIH Image combined with subtracting image filtering using Matlab software (The MathWorks, Natick, Mass., USA). The velocity of erythrocytes in individual segments of the peritubular capillaries, as representative of peritubular capillary flow, was analyzed using a program specifically designed for adaptation from the previously developed algorithm [12].

Human L-FABP Chromosomal Transgenic Mice

Human L-FABP transgenic mice, described previously elsewhere [13], were used for these experiments. Briefly, the genomic DNA of human L-FABP, including its promoter region (13 kb), was microinjected into fertilized eggs obtained from C57B/6 and CBA mice. We used ICR mice as the recipients of the transfected eggs. The resultant transgenic mice were backcrossed for more than nine generations onto C57B/6 mice to obtain homozygous

mutant mice on an inbred background. Only heterozygous L-FABP transgenic mice were used in this experiment. Male wild-type and L-FABP transgenic mice weighing 20–25 g were allowed food and water ad libitum. The animals were first anesthetized with a combination of ketamine hydrochloride 11.6 mg/100 g and xylazine hydrochloride 0.77 mg/100 g; then they were killed.

Measurement of Blood Urea Nitrogen

Blood urea nitrogen was measured using the urease-indophenol method (Urea NB kit; Wako Pure Chemical Industries) using a 96-well plate reader (SpectraMax; Molecular Devices, Sunnyvale, Calif., USA) and 570 nm wavelength.

Urinary N-Acetyl-β-D-Glucosaminidase (NAG)

NAG is rich in renal tubular epithelial lysosomes. An increase of NAG is the hallmark of tubular epithelial cell injury. Absorbance at 580 nm indicates the colorimetric reaction of *m*-cresol, which is generated by the hydrolytic reaction of sodio-*m*-cresolsulfonphthaleinyl with NAG [9]. This assay is commercially available; the entire process was conducted following the manufacturer's protocol (NAG test; Shionogi, Osaka).

Measurement of Human L-FABP by ELISA

Urinary and serum human L-FABP levels were measured using a sandwich ELISA kit following the manufacturer's protocol (CMIC, Tokyo). The coefficient of variation is within 10% when the intra-assay reproducibility was determined by the same sample eight times. The measurable range of this kit is between 4 and 400 ng/ml. This ELISA kit does not cross-react with murine L-FABP. Measurements were performed in duplicate.

Quantitative Evaluation of Renal Fibrosis

Formalin-fixed sections (2 μm) were stained using Masson's trichrome, which indicates fibrosis as blue. The area of interstitial fibrosis in the cortex was evaluated using the computer-aided evaluation program AIS (Fuji Photo Film, Tokyo), as described previously [14]. Viewed at ×200, ten randomly selected nonoverlapping fields ranging from the outer medulla to the cortical region were analyzed. The fibrotic areas stained in blue were depicted in digital images; then the percentage of the fibrotic area was calculated relative to the entire field area (percentage area). Glomeruli and large vessels were not included in the microscopic fields for image analyses. Scores of respective kidneys were averaged; scores of each animal were also averaged.

Immunohistochemical Analysis

Immunohistochemical staining of 2-μm paraffin sections was performed using indirect techniques. Biotin-free immunohistochemical staining using a horseradish-peroxidase-conjugated polymer system was conducted according to the manufacturer's protocols with the Histofine Simple Stain Mouse MAX-PO (Rat) kit (Nichirei, Tokyo). The deparaffinized sections were preincubated with 0.3% hydrogen peroxide for 15 min and incubated with a primary antibody overnight at 4°C, followed by polymer-conjugated anti-mouse IgG. Protease K treatment was necessary for anti-F4/80 antibody. Diaminobenzidine tetrahydrochloride (Nichirei) was used for the substrate-chromogen reaction followed by counterstaining with hematoxylin. Control sections were subjected to secondary antibody only (blank). Mounted preparations were examined under a light microscope (E600; Nikon, Tokyo). Images were captured using a CCD camera (DM-1200; Nikon). Image software AIS was also used for quantitative evaluation of F4/80-positive area.

Table 1. Effects of the different diets and meloxicam on systolic blood pressure

Diet and meloxicam	Systolic blood pressure, mm Hg
Normal diet (n = 5)	117.2 ± 2.4
Low-Na diet for 2 weeks (n = 5)	117.5 ± 4.5
Low-Na diet for 2 weeks and meloxicam for	
2 days (n = 4)	137.8 ± 6.7
4 weeks (n = 6)	153.0 ± 8.2

Statistical Analyses

Differences among experimental groups were detected using one-way ANOVA with Tukey's HSD post hoc test. Student's t test was applied to some experimental results. Values are expressed as mean ± SD; $p < 0.05$ was considered significant. Correlations between two indicators were evaluated using the Spearman rank test, and $r < 0.75$ was considered a significant correlation.

Results

Blood Pressure

The systolic blood pressure (table 1) of mice fed a normal diet (n = 5) was 117.2 ± 2.4 mm Hg, whereas that of mice fed a low-sodium diet for more than 2 weeks (n = 5) was unchanged with 117.5 ± 4.5 mm Hg. Mice administered meloxicam for 2 days on a low-sodium diet showed a significantly higher systolic blood pressure of 137.8 ± 6.7 mm Hg (n = 4, $p < 0.05$ vs. low-sodium diet alone); those that received it for 4 weeks exhibited a further increase to 153.0 ± 8.2 mm Hg (n = 6, $p < 0.05$ vs. low-sodium diet alone).

Urinary Indicators

During daily administration of meloxicam for 2 days (n = 5), urinary L-FABP adjusted by urinary creatinine was significantly increased at 24 h (98.3 ± 39.4 μg/g creatinine; $p < 0.05$ compared to the basal level of 12.8 ± 3.7 μg/g creatinine, n = 5) and was further increased at 48 h (207.3 ± 48 μg/g creatinine; $p < 0.05$ vs. basal level and vs. 24 h) (fig. 1). Serum L-FABP at the 48-hour time point was 27.8 ± 16.1 ng/ml, which was statistically indistinct from the basal level. Similar to the data for meloxicam, animals that were administered celecoxib on a low-sodium diet showed a significant increase of urinary L-

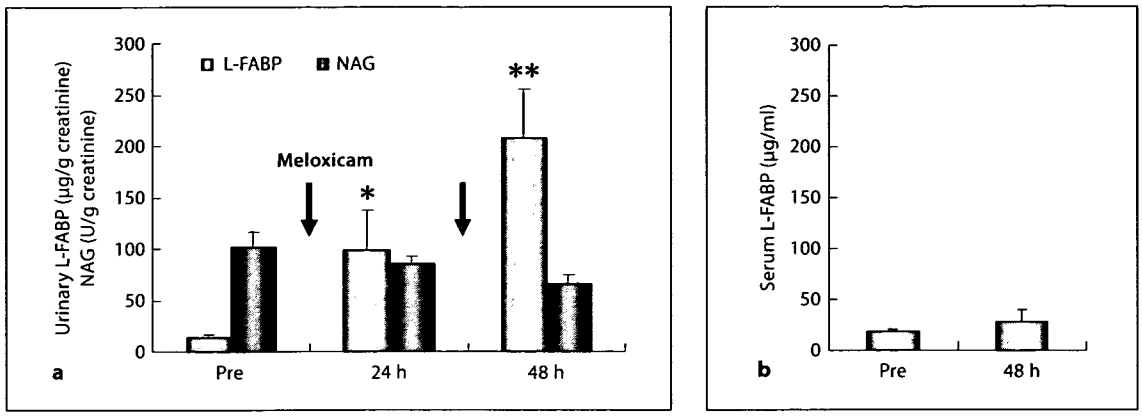

Fig. 1. Urinary L-FABP and NAG (**a**) and serum L-FABP levels (**b**). Animals were given a low-Na diet for 2 weeks before daily administration of meloxicam 2.5 mg/kg p.o. Both urinary L-FABP and NAG were standardized by urinary creatinine. * $p < 0.05$ pre vs. 24 h; ** $p < 0.05$ pre and 24 h vs. 48 h.

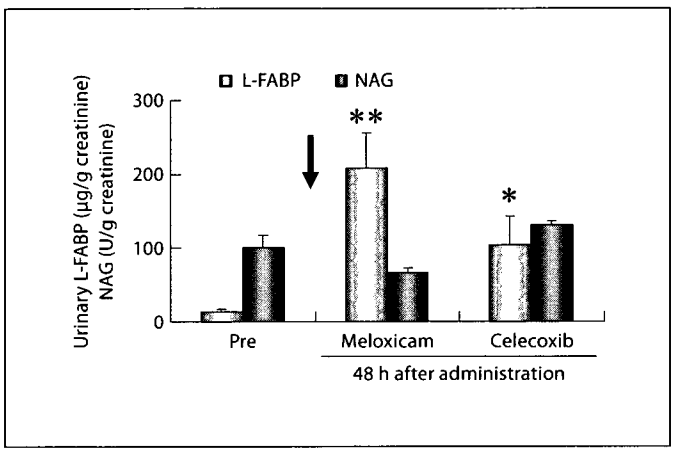

Fig. 2. Urinary L-FABP and NAG levels 48 h after starting either meloxicam or celecoxib. Animals were given a low-Na diet for 2 weeks before starting daily administration. Both urinary L-FABP and NAG were standardized by urinary creatinine. Each group includes 6 animals. * $p < 0.05$ celecoxib vs. basal level; ** $p < 0.05$ meloxicam vs. basal level or celecoxib.

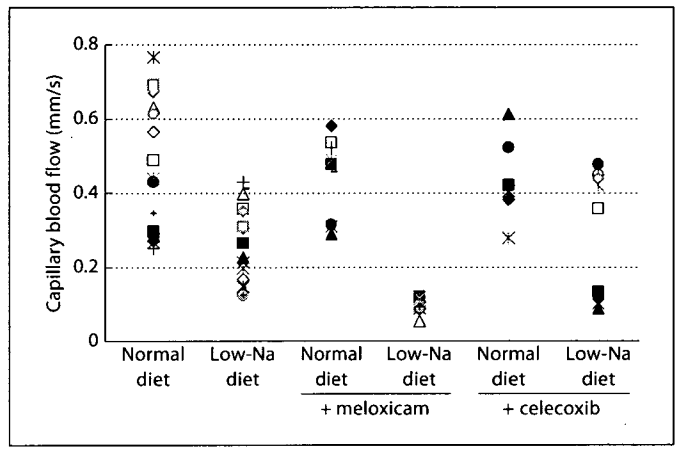

Fig. 3. Peritubular capillary blood flow measured using intravital CCD video. Low-Na diet denotes that animals were given a low-sodium diet 2 weeks before starting daily administration. Either meloxicam or celecoxib was administered for 2 days before analyses.

FABP: 103.7 ± 39.5 μg/g creatinine (fig. 2). Compared to urinary L-FABP, urinary NAG was insensitive (fig. 2).

Peritubular Capillary Blood Flow

Peritubular capillary blood flow was monitored next using an intravital CCD video system. As shown in figure 3, the peritubular capillary blood flow was reduced in the low-sodium diet group (0.27 ± 0.02 mm/s, n = 19) compared to animals fed a normal diet (0.47 ± 0.04 mm/s, n = 19), but this value did not indicate a statistically significant difference. Mice treated with either meloxicam or celecoxib showed values in between those of animals with normal and low-sodium diets. It is noteworthy that mice treated with meloxicam on a low-sodium diet showed a significant decrease of peritubular capillary blood flow (0.096 ± 0.004 mm/s, n = 19; $p < 0.05$ vs. normal diet, normal diet + meloxicam, and normal diet + celecoxib). Mice treated with celecoxib intriguingly showed a different response from that to meloxicam. Some animals showed a significant decrease of peritubu-

lar capillary blood flow compared to that of the normal-diet group, but others showed a blood flow equivalent to that of animals of the normal-diet group. Although we recently reported a significant correlation between the level of urine L-FABP and peritubular capillary blood flow [15], the observation described above reconfirmed that remarkable correlation.

Pathology

Both meloxicam and celecoxib were further administered for 4 weeks. Staining of kidneys using Masson's trichrome showed a marked increase of interstitial fibrosis in meloxicam-treated animals on a low-sodium diet compared with the animals on a normal diet (fig. 4a). Moreover, cellular infiltration into the interstitium was partially observed in meloxicam-treated animals on a low-sodium diet. Figure 4b shows results of quantitative analyses of fibrosis using image software (AIS), where the region of interest for fibrosis was preassigned in terms of the hue and contrast level. The small histological pictures shown above the bar graphs in figure 4b are representative AIS images. The total proportional area of fibrosis was significantly increased in both meloxicam-treated and celecoxib-treated animals on a low-salt diet compared with animals receiving a normal diet ($p < 0.05$, $n = 6$ in each group), although the level of fibrosis was mild to moderate. Interstitial cellular infiltration was observed at 4 weeks in kidneys harvested from meloxicam-treated animals receiving the low-sodium diet. Therefore, the F4/80 macrophage antigen antibody was applied for detection (fig. 5). The kidneys obtained from meloxicam-treated animals on a low-sodium diet showed a remarkable increase of interstitial infiltration of macrophages compared with animals receiving a normal diet ($p < 0.05$, $n = 5$ in each group). Those of the celecoxib-treated animals exhibited F4/80-positive cells at the vicinity of the peritubular region, but quantitative analyses demonstrated that the F4/80-positive staining area in celecoxib-treated animals was not as broad as that of the meloxicam-treated animals ($p < 0.05$, $n = 5$ in each group).

Blood Urea Nitrogen

The level of blood urea nitrogen at 4 weeks after administration of these preparations was not significantly altered and was similar among the animals ($n = 6$ in each group; fig. 6).

Urinary L-FABP Level and Fibrosis

Because animals treated with celecoxib on a low-sodium diet for 2 days showed different responses of peritubular capillary blood flow, depending on individual animals, we continued administration of celecoxib for 4 weeks and collected urine every week. Some animals showed increased urine L-FABP levels during 1 week after

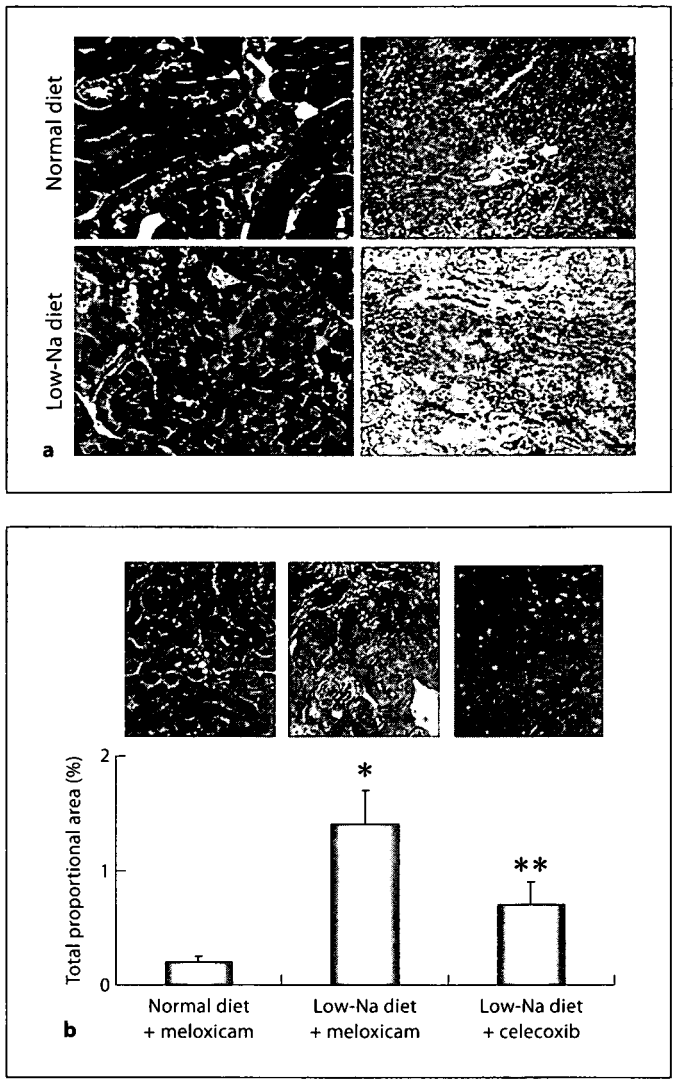

Fig. 4. a Renal histology of animals administered meloxicam for 4 weeks on either a normal or a low-Na diet. Left panels demonstrate Masson's trichrome. ×200. Right panels show periodic acid-Schiff. ×100. Blue staining in the lower left panel (Masson's) between tubules (arrows) demonstrates early development of fibrotic regions. The asterisk in the lower right panel (periodic acid-Schiff) shows the region of cellular infiltration. Bars depict 100 μm. **b** In the upper part representative images used for total proportional area analysis. The results are summarized in the bar graphs. Low-Na represents the preparation through prefeeding of a low-sodium diet for more than 2 weeks. Each group includes 6 animals. * $p < 0.05$ meloxicam low-Na vs. either meloxicam normal diet or celecoxib low-Na diet; ** $p < 0.05$ celecoxib low-Na diet vs. meloxicam normal diet.

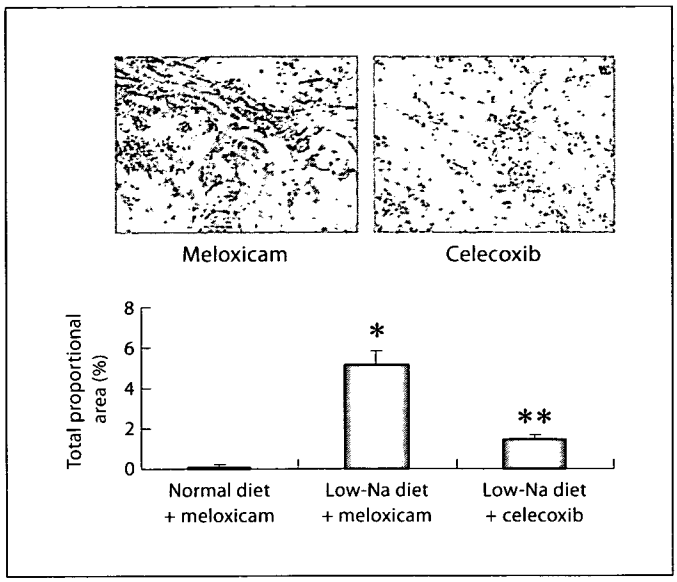

Fig. 5. Tubulointerstitial infiltrating F4/80-positive cells. Either meloxicam or celecoxib was administered for 4 weeks on a low-Na diet. * $p < 0.05$ meloxicam low-Na diet vs. either meloxicam normal diet or celecoxib low-Na diet; ** $p < 0.05$ celecoxib low-Na diet vs. meloxicam normal diet.

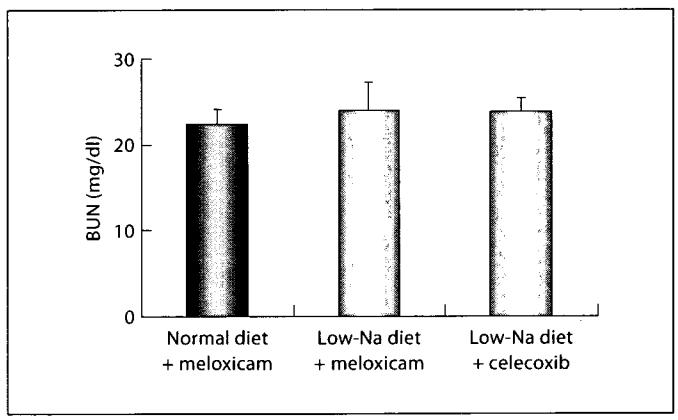

Fig. 6. Blood urea nitrogen (BUN) 4 weeks after starting either meloxicam or celecoxib. Each group includes 6 animals.

starting celecoxib, but others exhibited virtually no response (fig. 7a). Animals excreting higher amounts of urinary L-FABP than 50 μg/g creatinine during the follow-up period were defined as responders (n = 4). Those below that value were defined as nonresponders or low responders (n = 4). We evaluated the histological findings and quantified the degree of fibrosis 4 weeks later. As shown in figure 7b, the animals of the responder group showed a significant increase of their respective fibrotic regions compared to nonresponders ($p < 0.05$, n = 4 in each group). Correlations between urinary L-FABP and reciprocal of peritubular capillary blood flow 2 days after starting celecoxib are shown in figure 7c. Responders showed an increase of urinary L-FABP and reciprocal of peritubular capillary blood flow. In the responders, the more increased the reciprocal of peritubular capillary blood flow was, the more increased the urinary L-FABP level was. In nonresponders, both indicators showed no increase.

Discussion

The prescription of COX-2 inhibitors must be considered carefully, especially in geriatric individuals, though the selectivity of COX-2 theoretically better preserves renal function than regular NSAIDs. Chan et al. [16] investigated rheumatoid arthritis patients who had been prescribed either celecoxib or diclofenac and omeprazole for 6 months and found hypertension, peripheral edema, and renal failure in 24% of the celecoxib group and in 31% of the diclofenac and omeprazole group. Furthermore, renal failure was observed in 5.6% of the 144 celecoxib-treated patients and in 6.3% of those treated with diclofenac and omeprazole. The markets for these geriatric medications are saturated in the United States, but are increasing in Europe and in eastern Asian countries such as China, Korea, and Japan. Therefore, the chance of their prescription for pain relief is still increasing internationally. The renin-angiotensin-aldosterone system of such individuals is often at a higher level than that of younger individuals. This study was intended to examine the efficacy of urinary L-FABP to detect the risk of renal injury and to reveal chronic renal injury after intake of either meloxicam or celecoxib on a low-sodium diet, which easily upregulates the renin-angiotensin-aldosterone system. As expected, the peritubular capillary blood flow was significantly decreased in animals of the meloxicam and low-salt group 48 h after starting administration. The urinary L-FABP concentration of these animals had already increased at 24 h (fig. 1); the lower blood flow was established during the first 24 h. However, the other urine indicator, NAG, was insensitive to these hypoxic renal conditions (fig. 1, 2). We recently investigated living-related kidney transplantation and found a direct correlation between renal peritubular capillary flow and level of urinary L-FABP [15]. The evidence described here again confirmed urinary L-FABP as a biomarker of tubular hypoxic conditions. Moreover, animals that were adminis-

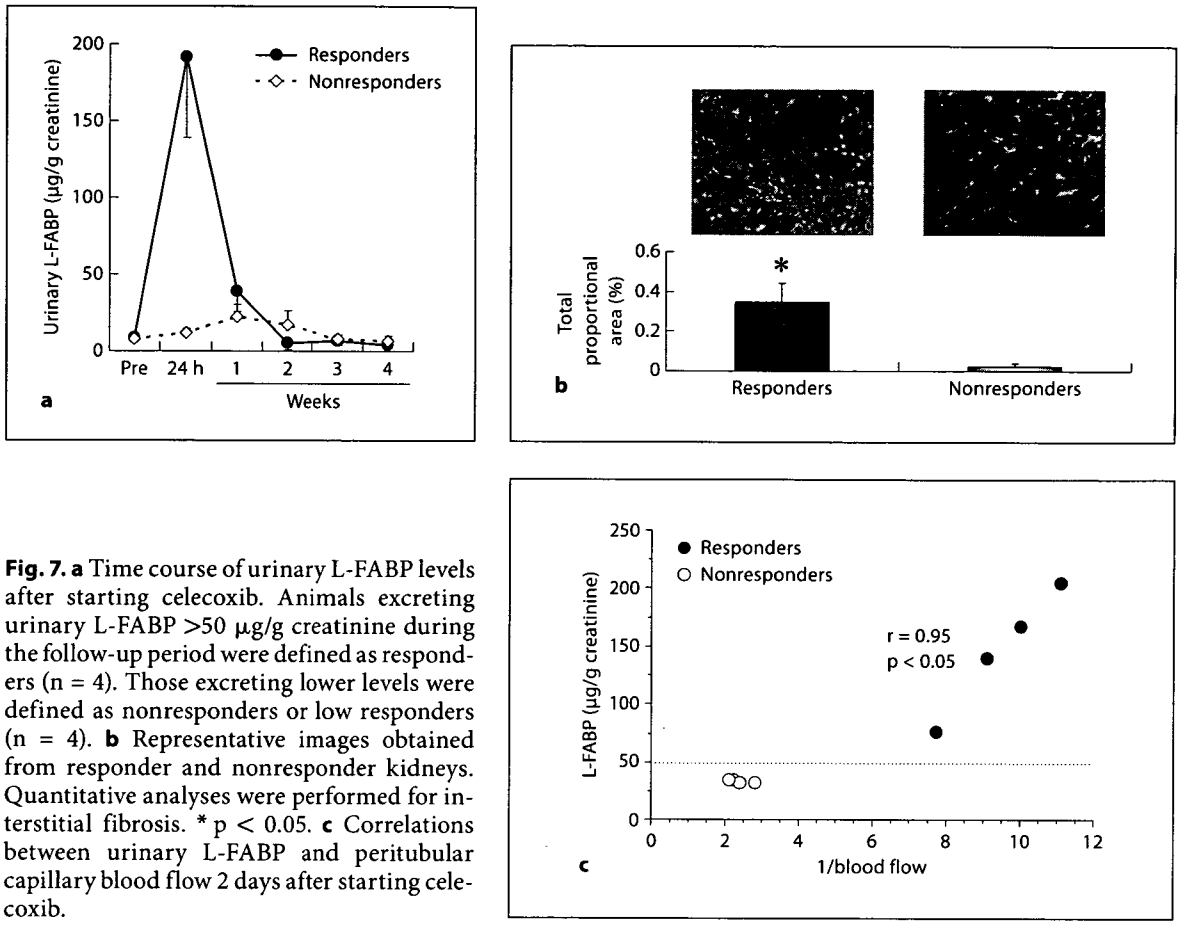

Fig. 7. a Time course of urinary L-FABP levels after starting celecoxib. Animals excreting urinary L-FABP >50 μg/g creatinine during the follow-up period were defined as responders (n = 4). Those excreting lower levels were defined as nonresponders or low responders (n = 4). **b** Representative images obtained from responder and nonresponder kidneys. Quantitative analyses were performed for interstitial fibrosis. * $p < 0.05$. **c** Correlations between urinary L-FABP and peritubular capillary blood flow 2 days after starting celecoxib.

tered meloxicam on a low-sodium diet for 4 weeks exhibited a fibrotic region at the tubular interstitium. That level was significantly increased compared to the normal-diet group (fig. 4). The cellular infiltration was apparent occasionally in animals treated with meloxicam on a low-sodium diet; the dominant population of these infiltrated cells consisted of macrophages (fig. 5). The meloxicam dosage in this experiment was in the nontoxic range, and the serum L-FABP level 48 h after starting daily meloxicam administration was not significantly increased. The effect of blood L-FABP derived from liver and/or intestine on urine is negligible, and the dynamics of urinary L-FABP is essential. Therefore, the initial urinary L-FABP level after starting meloxicam will be a promising biomarker to detect renal interstitial damage. Actually, L-FABP transgenic mice express human L-FABP, and the L-FABP ELISA system exclusively detects human L-FABP. Therefore, the above observations will be applicable directly to the prophylactic monitoring of prescriptions of this type of medication in humans.

Similarly, celecoxib, administered to the low-salt diet group, partially reduced peritubular capillary blood flow 48 h after starting daily administration. The renal interstitial fibrosis observed after 4 weeks was not comparable to that induced by meloxicam, but showed a significant increase compared to meloxicam administered together with a normal diet (fig. 4). Macrophage infiltration was not significantly increased, but F4/80-positive cells were visible between tubules. The dose of celecoxib used in this study is not in the toxic range and has often been used in previous studies [9]. The peritubular capillary blood flow was decreased in some animals that were administered celecoxib on a low-sodium diet. Therefore, we investigated whether that difference might be monitored by the level of urinary L-FABP. Celecoxib was administered daily on a low-sodium diet and urine was collected. As displayed in figure 7a, some animals excreted L-FABP into urine transiently within 2 weeks after starting daily celecoxib administration (responders), but others did not (nonresponders). Kidneys harvested at 4 weeks showed quantitatively remarkable differences of peritubular fi-

brosis between urinary L-FABP responders and nonresponders (fig. 7b). At 2 days after starting celecoxib, the decrease of peritubular capillary blood flow correlated with the increase of urinary L-FABP (fig. 7c). The transient elevation of the urinary L-FABP level reflects the initial damage demonstrated by the decrease of peritubular capillary blood flow. This initial change of the hemodynamics in the kidneys is pivotal and might further affect the development of mild interstitial fibrotic regions. The transient hypoxia despite the continuous administration of celecoxib might be because of some adaptation to hypoxia and further investigation will be necessary. Humans present a mixed population of responders and nonresponders whenever they are prescribed a certain medicine. Therefore, the observations from celecoxib and urinary L-FABP monitoring in this study might closely apply to a practical medical situation and be useful to distinguish between responders and nonresponders. To our knowledge, this is the first report providing evidence of a biomarker-predictable chronic COX-inhibitor-induced renal interstitial injury. It is reasonable to examine the humanized renal response to newly discovered compounds for potential drugs before starting clinical phase I trials, which will enable cost savings in pharmaceutical development. Exploring effective biomarkers and a suitable animal model representative of a certain pathophysiological condition will ensure the rapid translation of basic scientific discovery into new and better medical treatments, which is requested by the Critical Path Initiative Fact Sheet by the FDA 2006. The study described in this article will be a representative model for that mission.

Acknowledgments

This study was supported in part by grants from the Takeda Science Research Foundation (Osaka, Japan, to E.N.); the Cell Science Research Foundation (Osaka, Japan, to E.N.); Health and Labour Science Research Grants for Research on Human Genomes, Tissue Engineering, and Food Biotechnology, Ministry of Health, Labour and Welfare, Japan (No. 057100000661 to E.N., T.Y., and T.S.); the BioBank Japan Project on the Implementation of Personalized Medicine, MEXT (Ministry of Education, Culture, Sports, Science and Technology), Japan (No. 3023168 to E.N.); by Special Coordination Funds for Promoting Science and Technologies, MEXT, Japan (No. 1200015 to E.N.); by KAKENHI, MEXT, Japan (No. 19590935 to E.N. and T.S.); by NIH/NIDDK RO1-DK075976 (to D.P.), and by a Veterans Affairs Merit Award, USA (to D.P.).

References

1 Kramer HJ, Stinnesbeck B, Klautke G, Kipnowski J, Klingmueller D, Glaenzer K, Duesing R: Interaction of renal prostaglandins with the renin-angiotensin and renal adrenergic nervous systems in healthy subjects during dietary changes in sodium intake. Clin Sci (Lond) 1985;68:387–393.
2 Muther RS, Potter DM, Bennett WM: Aspirin-induced depression of glomerular filtration rate in normal humans: role of sodium balance. Ann Intern Med 1981;94:317–321.
3 Cryer B, Feldman M: Cyclooxygenase-1 and cyclooxygenase-2 selectivity of widely used nonsteroidal anti-inflammatory drugs. Am J Med 1998;104:413–421.
4 Vane JR, Bakhle YS, Botting RM: Cyclooxygenases 1 and 2. Annu Rev Pharmacol Toxicol 1998;38:97–120.
5 Gilroy DW, Colville-Nash PR, Willis D, Chivers J, Paul-Clark MJ, Willoughby DA: Inducible cyclooxygenase may have anti-inflammatory properties. Nat Med 1999;5:698–701.
6 Gabriel SE, Jaakkimainen L, Bombardier C: Risk for serious gastrointestinal complications related to use of nonsteroidal anti-inflammatory drugs. A meta-analysis. Ann Intern Med 1991;115:787–796.
7 Cheng HF, Wang JL, Zhang MZ, Miyazaki Y, Ichikawa I, McKanna JA, Harris RC: Angiotensin II attenuates renal cortical cyclooxygenase-2 expression. J Clin Invest 1999;103:953–961.
8 Cheng HF, Harris RC: Cyclooxygenases, the kidney, and hypertension. Hypertension 2004;43:525–530.
9 Engelhardt G, Bogel R, Schnitzler C, Utzmann R: Meloxicam: influence on arachidonic acid metabolism. II. In vivo findings. Biochem Pharmacol 1996;51:29–38.
10 Yamamoto T, Tada T, Brodsky SV, Tanaka H, Noiri E, Kajiya F, Goligorsky MS: Intravital videomicroscopy of peritubular capillaries in renal ischemia. Am J Physiol Renal Physiol 2002;282:F1150–F1155.
11 Matsumoto M, Tanaka T, Yamamoto T, Noiri E, Miyata T, Inagi R, Fujita T, Nangaku M: Hypoperfusion of peritubular capillaries induces chronic hypoxia before progression of tubulointerstitial injury in a progressive model of rat glomerulonephritis. J Am Soc Nephrol 2004;15:1574–1581.
12 Ogasawara Y, Takehara K, Yamamoto T, Hashimoto R, Nakamoto H, Kajiya F: Quantitative blood velocity mapping in glomerular capillaries by in vivo observation with an intravital videomicroscope. Methods Inf Med 2000;39:175–178.
13 Kamijo A, Sugaya T, Hikawa A, Okada M, Okumura F, Yamanouchi M, Honda A, Okabe M, Fujino T, Hirata Y, Omata M, Kaneko R, Fujii H, Fukamizu A, Kimura K: Urinary excretion of fatty acid-binding protein reflects stress overload on the proximal tubules. Am J Pathol 2004;165:1243–1255.
14 Noiri E, Nagano N, Negishi K, Doi K, Miyata S, Abe M, Tanaka T, Okamoto K, Hanafusa N, Kondo Y, Ishizaka N, Fujita T: Efficacy of darbepoetin in doxorubicin-induced cardiorenal injury in rats. Nephron Exp Nephrol 2006;104:e6–e14.
15 Yamamoto T, Noiri E, Ono Y, Doi K, Negishi K, Kamijo A, Kimura K, Fujita T, Kinukawa T, Taniguchi H, Nakamura K, Goto M, Shinozaki N, Ohshima S, Sugaya T: Renal L-type fatty acid-binding protein in acute ischemic injury. J Am Soc Nephrol 2007;18:2894–2902.
16 Chan FK, Hung LC, Suen BY, Wu JC, Lee KC, Leung VK, Hui AJ, To KF, Leung WK, Wong VW, Chung SC, Sung JJ: Celecoxib versus diclofenac and omeprazole in reducing the risk of recurrent ulcer bleeding in patients with arthritis. N Engl J Med 2002;347:2104–2110.

Original Article

A Water-Soluble Fullerene Vesicle Alleviates Angiotensin II–Induced Oxidative Stress in Human Umbilical Venous Endothelial Cells

Rui MAEDA[1),2)], Eisei NOIRI[1),3),4)], Hiroyuki ISOBE[1),2)], Tatsuya HOMMA[2)], Tamami TANAKA[4)], Kousuke NEGISHI[4)], Kent DOI[4)], Toshiro FUJITA[3),4)], and Eiichi NAKAMURA[1),2),5)]

A water-soluble fullerene vesicle based on the Buckminsterfullerene molecule ($Ph_5C_{60}K$, denoted as PhK) was explored to determine its effects on anti-oxidation of human umbilical endothelial cells (HUVEC) exposed to exogenous and endogenous reactive oxygen species (ROS). Hydrogen peroxide 0.05–0.25 mmol/L remarkably reduced the cellular viability of HUVEC. This reduction in viability was markedly improved when PhK 0.01–1 μmol/L was added simultaneously to the culture medium. The reduction of viability in HUVEC induced by angiotensin II (AII) 10^{-9} to 10^{-7} mol/L was improved by pretreatment with PhK 0.1 or 10 μmol/L 12 h before AII stimulation. The ROS indicator CM-H_2DCFDA demonstrated the efficacy of PhK 1 or 10 μmol/L in decreasing AII-induced ROS production to the level induced by the AII receptor blocker RNH-6470 20 μmol/L. The AII-induced peroxynitrite formation, as gauged using hydroxyphenyl fluorescein as a probe, was alleviated significantly by either pretreatment with PhK 0.1 or 1 μmol/L. Electron microscopy revealed intracellular localization of PhK in HUVEC after 12 h incubation. The PhK decreased the AII-induced apoptosis and lipid peroxidation processes as revealed by hexanoyl-lysine adduct formation. These observations show that the PhK water-soluble fullerene vesicle is promising as a compound controlling not only exogenous ROS, but also endogenous AII-mediated pathophysiological conditions. (*Hypertens Res* 2008; 31: 141–151)

***Key Words*: reactive oxygen species, endothelial cells, nano-compound, apoptosis**

Introduction

It has recently been suggested that angiotensin II (AII) is not simply an autacoid with hemodynamic and renal actions, but rather a biologically active mediator that imparts direct effects on endothelial and vascular smooth muscle cells. Actually, AII plays a key role in the initiation and amplification of pathobiological events leading to vascular disease. In addition, AII is a major mediator of oxidative stress and

From the [1)]Center for NanoBio Integration, [2)]Department of Chemistry, [3)]Department of Hemodialysis and Apheresis, [4)]Department of Nephrology and Endocrinology, The University of Tokyo, Tokyo, Japan; and [5)]Japan Science and Technology Agency, ERATO, Nakamura Functional Carbon Cluster Project, Tokyo, Japan.

Part of this study was supported by the NanoBio Integration Program, Ministry of Education, Culture, Sports, Science and Technology (MEXT), Japan (R.M., E.N., H.I., E.N.), by Health and Labour Sciences Research Grants for Research on Human Genome, Tissue Engineering Food Biotechnology from the Ministry of Health, Labour and Welfare, Japan (057100000661 E.N.), by a Grant-in-Aid for Scientific Research from the MEXT, Japan (19590935 E.N.), by the BioBank Japan Project on the Implementation of Personalized Medicine, MEXT, Japan (3023168 E.N.), by Special Coordination Funds for Promoting Science and Technologies, MEXT, Japan (1200015 E.N.), and by ERATO, JST, Japan (Nakamura Functional Carbon Cluster Project; E.N.).

Address for Reprints: Eisei Noiri, M.D., Department of Nephrology 107 Laboratory, University Hospital, The University of Tokyo, 7–3–1 Hongo, Bunkyo-ku, Tokyo 113–8655, Japan. E-mail: noiri-tky@umin.ac.jp

Received April 19, 2007; Accepted in revised form August 5, 2007.

reduces nitric oxide (NO) activity by activating NADH/NADPH oxidase (*1*), thereby generating superoxide anion ($O_2^{\cdot-}$) according to the reaction NADPH + $2O_2 \rightarrow 2O_2^{\cdot-}$ + $NADP^{+}$ + H^{+}. Found initially in phagocytic cells, NAD(P)H oxidase has also been identified in non-phagocytic cells such as fibroblasts (*2*), endothelial cells (*3*), vascular smooth muscle cells (*4*), renal mesangial cells (*5, 6*), and renal tubular cells (*7, 8*). The upregulation of NAD(P)H oxidase by AII has been demonstrated in aortic vascular smooth muscle (*9, 10*), afferent arterioles of the glomerulus (*11*), and endothelial cells. Reaction between the superoxide anion and nitric oxide will generate peroxynitrite, resulting in oxidative stresses that are highly damaging to endothelial cells. Moreover, studies using chronic kidney disease rodent models have suggested that AII receptor blockade has beneficial effects beyond mere blood-pressure lowering (*12, 13*). It would be of additional interest if AII were to generate superoxide independent of the AII receptor. Therefore, the reduction of AII-mediated oxidative stress presents one approach to control macro-vasculature and micro-vasculature remodeling and endothelial apoptosis (*14*).

Osawa hypothesized in 1970 that fullerenes were the third allotropic carbon form, following graphite and diamond. Because the corannulene molecular structure was a subset of a structure with a soccer ball–like shape, he hypothesized the existence of a full ball (*15*). In 1985, Osawa's prediction—which had been made in a local chemistry journal "*Kagaku*" in Japan and gone mostly unnoticed for over a decade—was rediscovered by Kroto *et al.* (*16*), who began the search anew, and the fullerene was finally isolated in 1990 by Krätschmer *et al.* (*17*). Among fullerenes, C_{60}, or the Buckminsterfullerene, is the smallest. As predicted, it resembles a soccer ball, comprising hexagons and pentagons with no two hexagons sharing an edge. This fullerene is naturally occurring, and commonly found in candle soot. The anti-oxidative potency of native C_{60} fullerenes has been reported by Krusic *et al.* (*18*). The spheroidal structure of C_{60} fullerenes, consisting of numerous interconnected double bonds, is highly reactive with oxygen free radicals. Therefore, the chemical capability to receive oxygen free radicals will be superior to that of known scavengers. Water-soluble fullerenes were first reported by Chiang *et al.* (*19*), Friedman *et al.* (*20*), and Tokuyama *et al.* (*21*). The solubility was secured by either allelic hydroxy or carboxylic acid functional groups synthesized on carbon atoms of the fullerene structure, as seen in fullerenol-1 ($C_{60}(OH)_nO_m$, n=18–20, m=3–7 hemiketal moieties). Subsequently, soluble fullerenes like fullerenol-1 were applied to life sciences. Furthermore, the electric paramagnetic resonance measurement demonstrated that fullerenol-1 virtually abolishes the •OH signal generated by hydrogen peroxide. It is also noteworthy that, by the addition of •OH radicals to the fullerenol-1 molecule, the spheroidal structure of C_{60} provided more stable adducts of C_{60}. In spite of these theoretical aspects implying an inert nature, accumulating evidence supports the notion that fullerenes have prooxidant characteristics (*22–25*). Most of these studies were performed using water-insoluble fullerenes, which are a very different chemical entity from the soluble group, and which must be used with caution due to their toxicity presumably secured during their extraction processes.

Two reports (*26, 27*) have described the anti-oxidative capabilities of water-soluble fullerenes, but none have described a water-soluble fullerene vesicle. Dugan *et al.* investigated the anti-oxidative capacity of water-soluble fullerenes *in vitro* and found that those capabilities differ depending on the chemical structure of the functional group on the surface (*28*). They demonstrated the efficacy of carboxyfullerenes in preventing neuronal death induced by serum deprivation or exposure to Alzheimer amyloid peptide ($A\beta_{1-42}$). We have developed a water-soluble fullerene vesicle of less than 100-nm diameter, which is potentially suitable for endocytotic incorporation, and which is expected to reduce both extracellular and intracellular oxidative stress much more efficiently than previous water-soluble fullerenes. This study, for the first time, examined that antioxidative fullerene-vesicle capability.

Methods

Materials

H_2DCFDA, a "dihydro" derivative of fluorescein, is readily oxidized back to the parent dye, and is thus commonly used as a fluorogenic probe to detect the generation of reactive oxygen species (ROS). A chlormethyl (CM-) derivative of H_2DCFDA, CM-H_2DCFDA, exhibits more specific fluorescence against ROS in live cells than other derivatives, and was therefore used in the present study. CM-H_2DCFDA was obtained from Molecular Probes Inc. (Eugene, USA). Daiichi Sankyo Co. Ltd. (Tokyo, Japan) provided the AII receptor blocker RNH-6270 (RNH; olmesartan) (*29*). For this study, hydroxyphenyl fluorescein (HPF; 2-[6-(4′-hydroxy)phenoxy-3H-xanthen-3-on-9-yl]benzoic acid) was acquired (Daiichi Pure Chemicals Co., Ltd., Tokyo, Japan). HPF does not react with nitric oxide, superoxide, or hydrogen peroxide, and thus responds more specifically to peroxynitrite and hydroxyl radical (*30*). Annexin V and propidium iodide were also obtained from Molecular Probes Inc. Alamar blue was obtained from Biosource International Inc. (Camarillo, USA). The oxidized form of Alamar blue, which has little intrinsic fluorescence, becomes reduced in viable cells. Consequently, the reduced form of Alamar blue is highly fluorescent, and the cellular viability can be quantified by the extent of this conversion. All other chemicals were purchased from Wako Pure Chemical Industries Ltd. (Osaka, Japan) unless otherwise specified.

Fabrication of a Water-Soluble Fullerene Vesicle

The method used to generate water-soluble fullerenes was detailed previously by our group (*31, 32*). In brief, the R

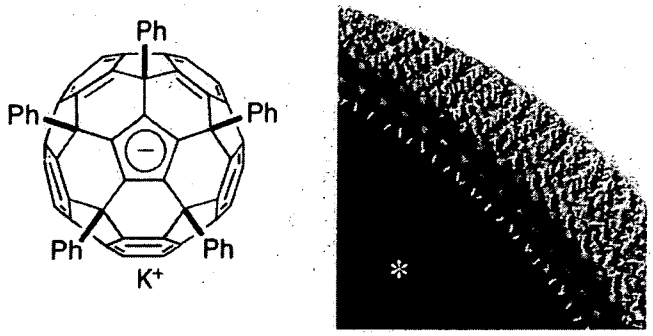

Fig. 1. *Structure of water-soluble fullerene PhK. The three-dimensional structure of fullerene is depicted in the left panel. The estimated outer radius of the fullerene vesicle consisting of PhK is 17.6 nm. Some vesicles shown in the right panel display a bilayer structure in aqueous solution. The asterisk indicates the interior of the fullerene vesicle. Details of the macro-structure are described in our previous report (32).*

(functional group) is substituted with C_6H_5, namely phenyl (penta-) substituted fullerene cyclopentadienide ($Ph_5C_{60}K$, abbreviated as PhK), and attains hydrophobic capabilities. The PhK bilayer vesicle consists of a monoanionic PhK molecule in aqueous solution; its outer shell radius is theoretically calculated as 17.6 nm in water. The micro-chemical structure of PhK is depicted in Fig. 1 (left), along with the putative bilayer structure (right). The structure of the PhK bilayer vesicle was reported previously by our group (*32*).

Cell Culture

Human umbilical venous cells (HUVEC) was obtained from the Health Science Research Resource Bank (HSRRB, Osaka, Japan) and maintained in the defined medium with endothelial supplementation (EGM2 Bullet Kit; Clonetics Corp., San Diego, USA). Endothelial cells were lifted with 0.05% trypsin–0.53 mmol/L EDTA (Gibco BRL, Gaithersburg, USA) and washed. Then 2×10^4 cells/well were seeded in each well of a 96-well plate (Corning Inc., Corning, USA). All experiments were performed using HUVEC between passages 3 and 6.

Cell Viability Assay

The Alamar blue assay is designed to measure cell viability simply, sensitively, and rapidly. The sensitivity and specificity of this dye for measuring cell viability and cytotoxicity are comparable to those of MTT (3-(4,5-dimethylthiazol-2-yl)-2,5-diphenyl-tetrazolium bromide) assay (*33*). Alamar blue is equivalent to non-fluorescent resazurin in oxidized form. Alamar blue appeared very stable in an already "reduced" CO_2-buffered medium. The presence of living cells allowed the reduction of dye through respiration-dependent metabolic activity in which electrons were donated to Alamar blue. The reduced form of Alamar blue is equivalent to resorufin, which has a pinkish fluorescence, and therefore reflects the cellular viability. Among a wide variety of reductases, diaphorase has been identified as the enzyme that is most likely to be responsible for the reduction of resazurin in semen (*34*). Matsumoto *et al.* also demonstrated the diaphorase-dependent reduction of resazurin to resorufin *in vitro* (*35*). Therefore, the level of resofurin will partially reflect the physiological tonus of nitric oxide in endothelial cells.

The HUVEC, seeded in a 96-well microplate (Corning Inc.) at a density of 2×10^4 per well, were capable of creating a cell monolayer after overnight incubation (15 h) and exposure to hydrogen peroxide alone or in combination with the water-soluble fullerene vesicle (PhK) until 8 h of the indicated concentration. To examine cell viability, HUVEC were loaded with 10% Alamar blue. In each experiment, Alamar blue fluorescence was measured on four separate cell monolayers at an excitation wavelength of 544 nm and an emission wavelength of 590 nm using a fluorescent microplate reader (fMax; Molecular Devices Corp., Sunnyvale, USA) and analyzed using software (SoftMax Pro; Molecular Devices Corp.). The experiment was repeated four times. Then HUVEC were preincubated with PhK at 0.1 or 10 μmol/L for 12 h, and subsequently stimulated by the indicated concentration of AII for 8 h. Cellular viability was expressed using the index of percent viability (% viability) against the timed control cells of the same preparation without agonist. A negative control for PhK was established by addition of vehicle (saline) alone instead of PhK. Similarly, RNH was used as a positive control in the AII experiment.

Fluorescence Measurement of Intracellular ROS and Peroxynitrite Production

To measure intracellular ROS production, the HUVEC were loaded on a 96-well fluorescent plate (Corning Inc.) with 10 μmol/L CM-H_2DCFDA for 30 min at 37°C in the dark. Under each experiment, fluorescence of CM-H_2DCFDA was measured on four separate cell monolayers using an excitation

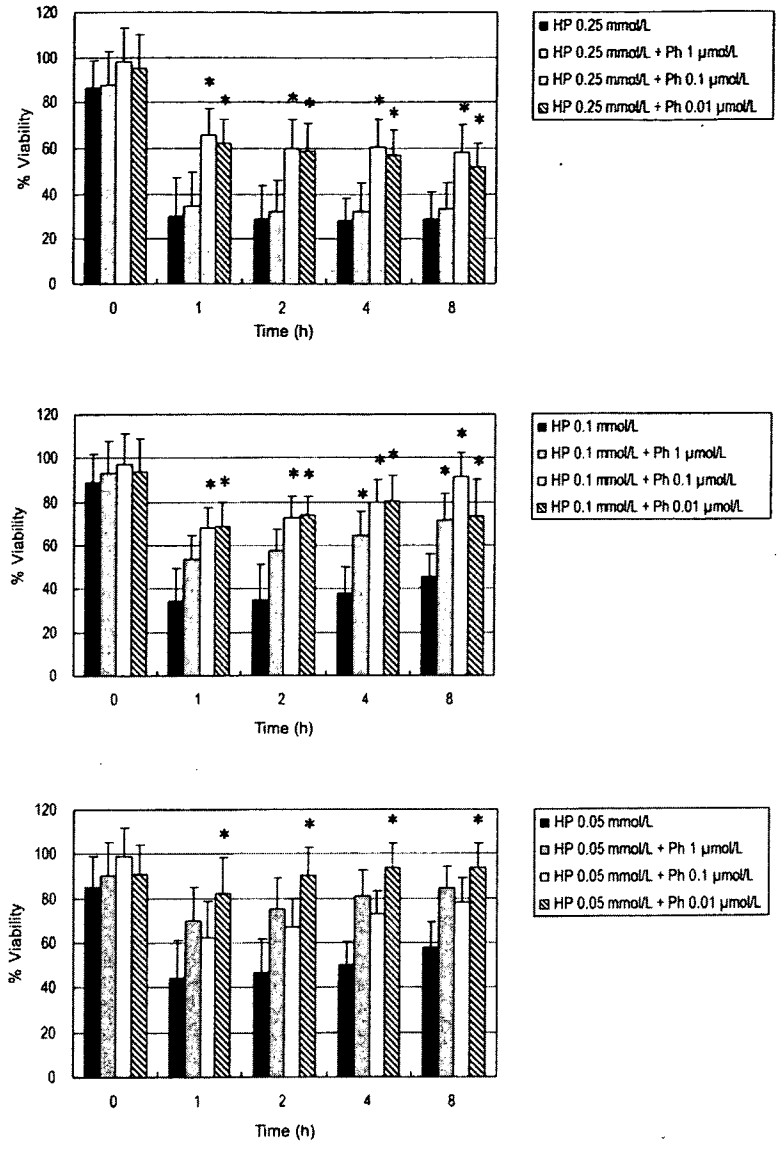

Fig. 2. *PhK improved cellular viabilities against exogenous oxidative stress. Different doses of hydrogen peroxide (HP) and PhK were administered to HUVEC. Cell viabilities were monitored serially at 0, 1, 2, 4, and 8 h time-points. The vertical bar represents % viability. Asterisks denote $p < 0.05$ compared to the positive control.*

wavelength of 485 nm and an emission wavelength of 538 nm with a fluorescence microplate reader (fMax). The HUVEC were exposed to hydrogen peroxide alone at a concentration of 0.10 mmol/L and in combination with fullerenes at concentrations of 0.1 μmol/L, 1 μmol/L, and 10 μmol/L. Experiments were performed for 1 h. Similarly, AII 10^{-7} mol/L was inoculated onto HUVEC after pretreatment with fullerene at the concentrations of 0.1 μmol/L, 1 μmol/L, and 10 μmol/L, as described above, and left for 1 h. The dose-dependency of AII was also monitored for intracellular ROS production. After referring to previous reports of *in vitro* studies, RNH was used at 20 μmol/L concentration (*36–38*). The experiment was repeated four times.

The AII-induced peroxynitrite generation was examined further in HUVEC seeded on a 96-well fluorescent plate. Preincubation of PhK at 0.1 μmol/L or 1 μmol/L was conducted for 12 h, as described above. The peroxynitrite formation was measured using the peroxynitrite-dependent oxidation of dihydrorhodamine-123 to rhodamine-123 using a concentration of 5 μmol/L (*39*). After 24-h incubation, the fluorescence of rhodamine-123 was measured at an excitation wavelength of 500 nm and emission wavelength of 536 nm. Alternatively, peroxynitrite and hydroxyl radical generation were measured using hydroxyphenyl fluorescein (HPF) 10 μmol/L at an excitation wavelength of 485 nm and an emission of 535 nm, where HPF is non-fluorescent until it reacts with the perox-

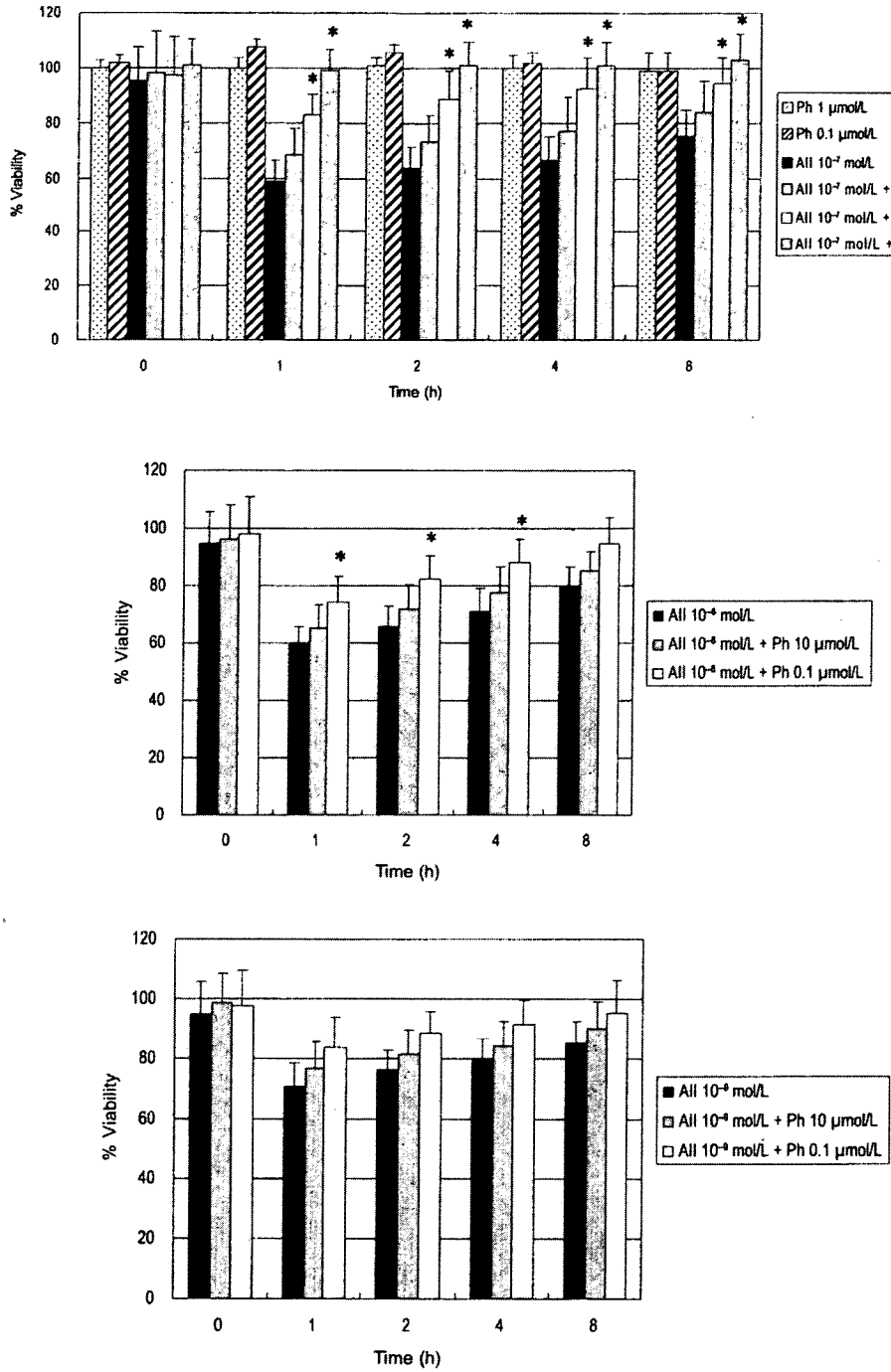

Fig. 3. *PhK improved cellular viabilities against endogenous oxidative stress. Different doses of AII and PhK were administered to HUVEC. Cell viabilities were monitored serially at 0, 1, 2, 4, and 8 h time-points. The vertical bar represents % viabilities. Asterisks denote $p < 0.05$ compared to the positive control.*

ynitrite or related hydroxy radicals. All experiments were performed in quadruplicate, and the experiment was repeated four times.

Flow Cytometry Analysis

Either hydrogen peroxide or AII in combination with PhK was administered to HUVEC monolayers according to the protocols described above. The HUVEC 1×10^6 cells/mL were suspended into 500 μL pre-warmed (37°C) PBS

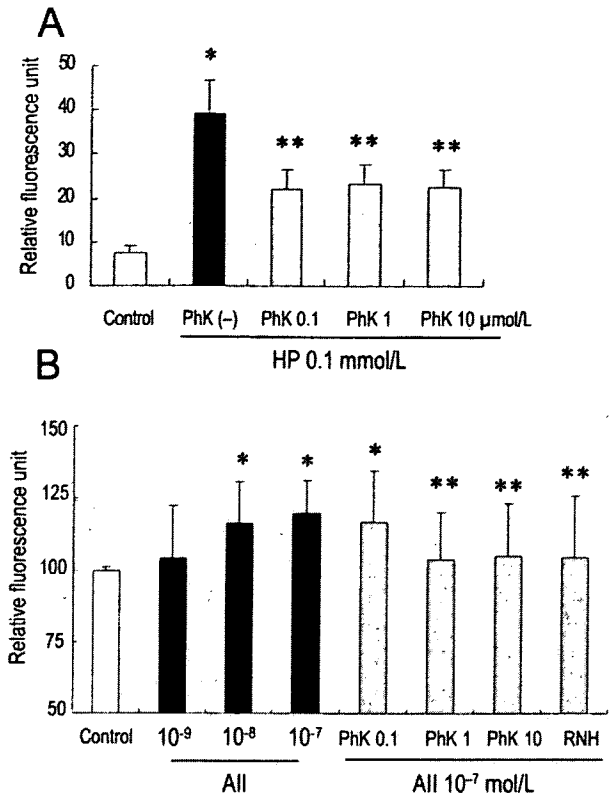

Fig. 4. *PhK reduced exogenous and endogenous oxidative stress. One hour of stimulation with hydrogen peroxide (HP) 0.1 mmol/L was used as an exogenous oxidative stressor (A). Similarly, 1 h of stimulation with the indicated dose of angiotensin II (AII) was used as an endogenous oxidative stressor (B). Exogenous and endogenous ROS were measured using CM-H_2DCFDA. The control cells were treated with vehicle. A single asterisk denotes a significant increase ($p < 0.05$) vs. the control group. The double asterisk denotes a significant decrease ($p < 0.05$) vs. AII 10^{-7} mol/L stimulation.*

(Sigma-Aldrich Corp., St. Louis, USA) supplemented with 5% FBS after trypsinization and washing.

Annexin V 5% was added to the cell suspension, and then incubated at 37°C for 15 min following the manufacturer's instructions. Subsequently, propidium iodide was added at a concentration of 1 μg/mL and flow cytometry was performed using FACScan (BD Biosciences Immunocytometry Systems, San Jose, USA) at a 488 nm excitation wavelength and emission filters of 530 nm (FL-1 channel) and 675 nm (FL-3 channel). Data were analyzed using Cell Quest pro (BD Biosciences). Annexin V detected apoptotic and necrotic cells at the FL-1 high positive area or FL-1 and FL-3 double-positive areas.

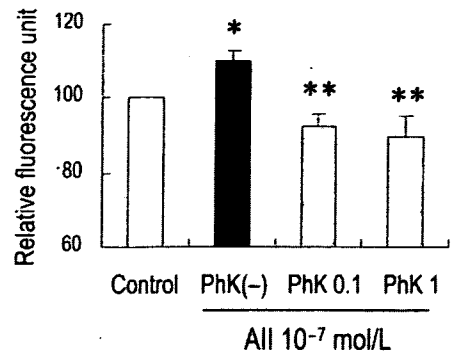

Fig. 5. *AII-induced peroxynitrite and hydroxyl radical generation and the efficacy of PhK. HPF was used for detecting peroxynitrite and/or hydroxyl radical. A single asterisk denotes a significant increase of peroxynitrite generation in the AII without PhK group (PhK(–), $p < 0.05$) compared to the control group. The AII-induced increase of peroxynitrite was alleviated significantly when PhK was added to the medium (double asterisks; $p < 0.05$).*

Preparation for Transmission Electron Microscopic Examination

The HUVEC grown on cover slips to semi-confluence were incubated with PhK 10 μmol/L for 12 h, washed three times using PBS, and fixed using 2.5% glutaraldehyde (Electron Microscopy Sciences, Ft. Washington, USA) for 45 min at 4°C. After washing three times with PBS, samples were immersed in 1.5% oxidized osmium for 1 h at 4°C. Post-fixation was performed using 2% paraformaldehyde with 2.5% glutaraldehyde in PBS (pH 7.1) for 20 min and then the samples were dehydrated. Cells on cover slips were transferred to Epon under mild heating. After ultrathin sectioning and post-fixation by uranium acetate and lead citrate, the transmission electron microscopic (TEM) (H-1000; Hitachi Ltd., Tokyo, Japan) examination was performed.

Immunocytochemical Analysis for Hexanoyl-Lysine Adducts Formation

The HUVEC grown in a slide chamber (BD Falcon, Franklin Lakes, USA) were stimulated using AII 10^{-7} mol/L in the presence or absence of PhK 1 μmol/L. Monoclonal antibody for hexanoyl-lysine (HEL; JaICA, Shizuoka, Japan) adducts was applied to the cell monolayer at a dilution of 1 to 200 after fixation using 2% glutaraldehyde and regular blocking procedures. The following staining was performed using a Vectorstain ABC system (Vector Laboratories Inc., Burlingame, USA). For substrate-chromogen reaction, Vector Red (Vector Laboratories Inc.) was used according to the manufacturer's protocol. Mounted preparations were examined using light microscopy (Nikon E600; Nikon Corp., Tokyo, Japan). Images were captured using a CCD camera

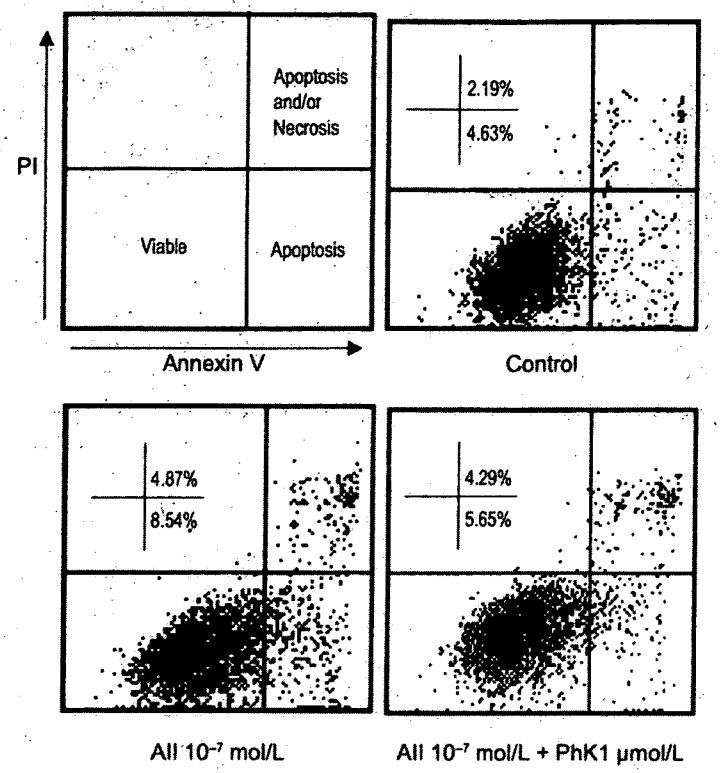

Fig. 6. *AII-induced cellular apoptosis and the efficacy of PhK. The upper left panel shows a map of the cellular distribution. AII 10^{-7} mol/L was added 1 h before measurement. Percentages of "Apoptosis and/or Necrosis" and "Apoptosis" are indicated in each panel.*

(DXM1200F; Nikon Corp., Tokyo, Japan).

Statistical Analyses

The results are expressed as the means±SD. The differences among experimental groups were detected using ANOVA with Tukey's HSD post hoc analysis. Values of $p<0.05$ were considered to indicate statistical significance.

Results

When HUVEC were subjected to exogenous oxidative stress by addition of hydrogen peroxide at concentrations of 0.05 mmol/L, 0.1 mmol/L, and 0.25 mmol/L for 8 h, cellular metabolic viability 1 h after the addition was decreased markedly to about 25% (at 0.25 mmol/L), 35% (0.1 mmol/L), and 45% (0.05 mmol/L) (Fig. 2). These decreases were prolonged for 8 h, but partial improvement in viability was apparent in the hydrogen peroxide 0.05 mmol/L and 0.1 mmol/L groups when PhK was added at a concentration between 0.01 and 1 μmol/L. Similarly, AII-induced reduction of metabolic activity was observed at 2 h after AII addition at concentrations between 10^{-7} and 10^{-9} mol/L (Fig. 3); this decrease was gradually reversed from between 2 and 8 h after AII addition. The decreases in metabolic activity were also greatly ameliorated when the cells were pretreated with PhK at concentrations of 0.1 μmol/L and 10 μmol/L.

The level of oxidative stress was measured using the fluorescent probe CM-H_2DCFDA. Hydrogen-peroxide 0.1 mmol/L–induced ROS were increased markedly from 4.6±0.7 (mean±SD) relative fluorescent units (rfu) in the vehicle group to 39.4±3.6, which was detected clearly using CM-H_2DCFDA. The increase was significantly less ($p<0.01$) for hydorogen peroxide 0.1 mmol/L + PhK 0.1 μmol/L (to 22.4±2.1 rfu), for hydorogen peroxide 0.1 mmol/L + PhK 1 μmol/L (to 23.5±2.2 rfu), and for hydorogen peroxide 0.1 mmol/L + PhK 10 μmol/L (to 22.6±2.2 rfu) (Fig. 4A). Then, AII-induced ROS generation was detected dose-dependently at concentrations of 10^{-7} mol/L and 10^{-9} mol/L using CM-H_2DCFDA. The remarkable increase in ROS production that was apparent in the cells treated with AII 10^{-7} mol/L (to 120.0±11.1 rfu) was reduced considerably by pretreatment with PhK 1 μmol/L (to 103.7±16.6 rfu) or 10 μmol/L (to 105.2±18.0 rfu), and these reduced levels were similar to that following treatment with the AII receptor blocker RNH (104.4±21.5) (Fig. 4B). Furthermore, AII-induced peroxynitrite generation *via* the reaction

$$O_2^{\cdot-} + NO \rightarrow ONOO^{-}$$

was detected after addition of AII at concentrations between

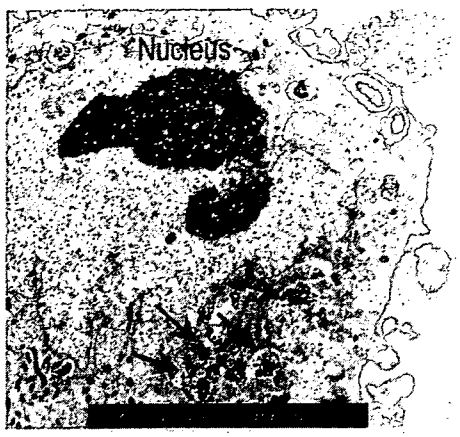

Fig. 7. *Intracellular localization of PhK. This TEM image was captured at 8,000× magnification. Arrows denote electron-dense PhK granules in the cytoplasmic region.*

10^{-7} and 10^{-9} mol/L using rhodamine 123, together with related oxidants. Compared to vehicle-treated cells, peroxynitrite-mediated oxidation was increased 1.9-fold in AII 10^{-7} mol/L–treated cells, 1.7-fold in 10^{-8} mol/L–treated cells, and 1.4-fold in 10^{-9} mol/L–treated cells. These increases were inhibited somewhat by 1 μmol/L PhK: 1.5-fold inhibition was observed in cells treated with AII 10^{-7} mol/L, 1.4-fold inhibition in cells treated with AII 10^{-8} mol/L, and 1.2-fold inhibition in cells treated with AII 10^{-9} mol/L. Next, HPF was used for the AII 10^{-7} mol/L cell preparation as a representative fluorescent indicator for peroxynitrite production. AII 10^{-7} mol/L markedly increased the fluorescence level of HPF, and this increase was decreased significantly by pretreatment with PhK 0.1 μmol/L or 1 μmol/L (Fig. 5).

The combination of Annexin V with propidium iodide is suitable to evaluate apoptosis *in vitro*. Compared to the control, AII 10^{-7} mol/L provoked cellular apoptosis in HUVEC; that induction was reduced by addition of PhK 1 μmol/L (Fig. 6; representative data of three experiments).

Because the AII-induced endogenous oxidative stress was decreased in HUVEC, intracellular incorporation of PhK into HUVEC was investigated using TEM analysis, which clarified the cytoplasmic localization of dense fullerene particles; that image was obtained after 24 h of incubation (Fig. 7).

Typically, ROS will affect the cell membrane, degrading it into arachidonic acid and linoleic acid, where lipid hydroperoxides are formed enzymatically during oxidative stress from 5-lipoxygenase (5-LOX), 15-LOX, cyclooxygenase-1 (COX-1), and COX-2. Both 15-LOX and COX-2 convert linoleic acid into the prototypic *n*-6 polyunsaturated fatty acid (PUFA) hydroperoxide. The major products from oxidized fatty acids are the esterified forms of 9- and 13- hydroxyl/hydroperoxy derivatives of linoleic acid. Furthermore, ROS-derived lipid hydroperoxides break down to form the α,β-unsaturated aldehyde genotoxins, 4-oxo-2-nonenal, 4-hydroxy-2-nonenal, and 4,5-epoxy-2(E)-decenal. Osawa and coworkers recently found that 13-HPODE bound covalently to proteins (*40*). The ROS-derived lipid-hydroperoxides are therefore capable of damaging cellular macromolecules such as DNA and proteins to form HEL, the lipid hydroperoxide–modified lysine residues. A monoclonal antibody raised against HEL adducts is therefore the representative oxidative stress marker for the earlier stages of the lipid peroxidation process. Figure 8 illustrates the AII-induced lipid peroxidation of HUVEC as visualized using anti-HEL antibody. The HEL adducts formation appeared in the cytoplasmic region, as shown in red in the image, when HUVEC were stimulated by AII 10^{-7} mol/L for 3 h. This finding was alleviated in the presence of PhK 1 μmol/L.

Based on the above results, PhK quenched $O_2^{\cdot-}$ derivates from NAD(P)H oxidase, and stopped prolongation of the $O_2^{\cdot-}$-mediated radical chain reaction; reaction with nitric oxide, lipid, mitochondrial DNA, and amino acid in protein. Those quenching will protect cells from apoptosis.

Discussion

This study demonstrated the ability of a water-soluble fullerene vesicle (PhK) to reduce both exogenous and endogenous oxidative stress. Exogenous oxidative stress often occurs with acute injury—*e.g.*, in tissue ischemia reperfusion, multiple organ failure (MOF), and inflammatory diseases such as systemic inflammatory response syndrome (SIRS). Endogenous oxidative stress is more often associated with chronic pathophysiological conditions, which are characterized by chronic endothelial dysfunction in both macro-vascular and micro-vascular systems. This is especially true of such pathophysiological conditions as hypertension, arteriosclerosis, ischemic heart disease, diabetes mellitus, and chronic kidney disease. In other words, endogenous oxidative stress is more closely related to metabolic syndrome and is presumably more important for preventive medicine. Endothelial nitric oxide affects the vasodilation of vascular smooth muscle. The level of endothelial nitric oxide is often mitigated by AII-dependent superoxide generation by NAD(P)H oxidase in endothelial cells (*3*). Consequently, a decrease of nitric oxide by superoxide definitely increases vascular tonus. Therefore, the influence of AII-induced oxidative stress is crucial for control of the diseases described above.

The efficacy of water-soluble fullerenes in reducing oxidative stress has been reported for polyhydroxylated fullerenes, carboxyfullerenes, and hexasulfobutyl[60]fullerenes. Polyhydroxylated fullerenes synthesized by Lai *et al.* were applied to a canine intestinal ischemia-reperfusion model (*41*). Polyhydroxylated fullerenes were effective at decreasing tissue conjugated diene content; which is an index of lipid peroxidation. The tissue malondialdehyde level was also decreased in a polyhydroxylated fullerene group, and the glutathione system was preserved. Similarly, carboxyfullerenes with a very large electronegative center were effective at inhibiting neuronal iron-induced oxidative stress (*42*); hexa-

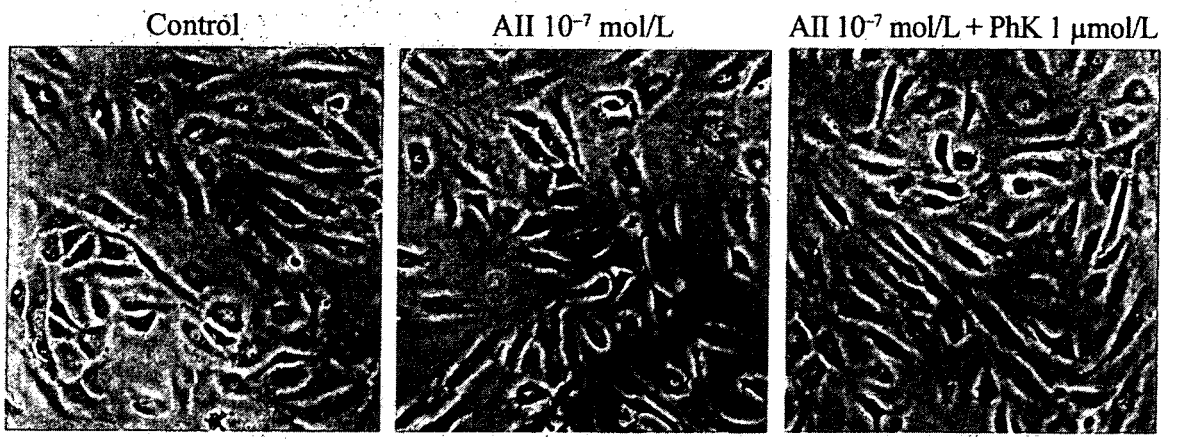

Fig. 8. *Immunocytochemical detection of HEL induced by AII, and efficacy of PhK. HUVEC stimulated by AII 10^{-7} mol/L for 3 h were examined immunocytochemically using monoclonal anti-HEL antibody. The HEL addcuts formation that was detectable in the cytoplasmic region as red signals was prohibited by administration of PhK 1 μmol/L.*

sulfobutyl[60]fullerenes, which consist of the six sulfobutyl functional group, were protective against oxidation of low-density lipoprotein (*43*). On the other hand, accumulated evidence exists to support prooxidant characteristics of fullerenes (*22–25*). Nonetheless, most of these studies investigated the non water-soluble type. Nagano *et al.* reported singlet oxygen generation from C_{60} fullerenes (*23*), and Satoh *et al.* demonstrated that daimonic acid C_{60} reduces nitric oxide–induced vasodilatation (*24*). Tsuchiya *et al.* reported that the ROS generated by C_{60} interrupts embryonic differentiation, thereby inducing anomalies (*25*); it also exhibits mutagenicity *via* lipid peroxidation (*44*). Furthermore, a recent report from Oberdörster *et al.* suggests the injurious nature of this molecule to marine organisms: they inoculated C_{60} fullerene into water at concentrations of 0.5 ppm and found that largemouth bass suffered a 17-fold increase in lipid peroxidative cellular damage in brain tissue after 48 h (*45*). Clearly, fullerenes have a dual nature, exhibiting both beneficial effects and malign toxicities. Standardization for the material-evaluation of fullerene is therefore required, as we recently suggested (*46*).

The pattern of fullerenes quenching singlet oxygen ($^1O_2$) is chemically dependent on their 30 carbon-carbon double bonds (C=C) (*18*, *47*). That mechanism, covalent double bonds reacting with $^1O_2$ through the charge transfer process, is often observed in other well known antioxidants, such as carotenoids (*48–50*) and flavonoids (*51*). In addition, the overall antioxidant and cell-protective capabilities of fullerenes are greater than those of vitamin E (*52*), and the $O_2^{\cdot-}$-quenching capabilities are equivalent to those of ascorbic acid and thiourea (*53*). It is always an issue that these antioxidants exhibit dual characteristics of both free radical generators and quenchers (*54*). Fullerene derivatives are no exception. However, PhK, which has phenyl groups located at the polar head of C_{60}, shows amphiphilicity and produces a bilayer vesicle consisting of 12,700 units of PhK, similar to a lipid bilayer (*32*). In fact, PhK differs from previously reported fullerene derivatives from a structural point of view. The hydrophobic sites, which consist of carbon double bonds and which react with radical species, are secured inside the bilayer (Fig. 1; right). Therefore, if radical chain reactions occur, the reaction might be prolonged inside the vesicle. For that reason, the countervailing radical generator effect that is often seen in antioxidants is inferred to be negligible in PhK.

The cytotoxicity of PhK must be investigated in greater detail in future studies, since PhK can be incorporated into the cytoplasmic region of endothelial cells, as shown by TEM; for that reason, the PhK vesicle might be effective for ameliorating the endogenous oxidative stress induced by AII. We found no cytotoxicity imparted by the dosage of PhK used in this study. The results of this study clarify that PhK is effective for reducing exogenous and endogenous oxidative stress *in vitro*. However, dose-dependency of PhK was not observed within the concentration range used in our experiment. Based on its chemical structure, PhK will never aggregate in pure water within the range of 1 to 10 μmol/L. Nevertheless, the higher electrolyte concentration in culture medium definitely induces aggregation of PhK at the nano-level, which mitigates the higher anti-ROS capability of PhK in higher concentration. For that reason, dose-dependency was not seen in our experiment.

AII-induced superoxide generation is inhibitable by PhK. This capability was shown to be effective at reducing the effects of the earlier stages of the lipid peroxidation process and thereby decreasing the level of cellular apoptosis. Additional studies will be needed to confirm the applicability of PhK to controlling AII-related pathophysiological conditions such as hypertension, atherosclerosis, ischemic heart disease, chronic heart failure, and chronic kidney disease.

References

1. Griendling KK, Minieri CA, Ollerenshaw JD, Alexander RW: Angiotensin II stimulates NADH and NADPH oxidase activity in cultured vascular smooth muscle cells. *Circ Res* 1994; **74**: 1141–1148.
2. Meier B, Jesaitis AJ, Emmendorffer A, *et al*: The cytochrome b-558 molecules involved in the fibroblast and polymorphonuclear leucocyte superoxide-generating NADPH oxidase systems are structurally and genetically distinct. *Biochem J* 1993; **289** (Pt 2): 481–486.
3. Bayraktutan U, Blayney L, Shah AM: Molecular characterization and localization of the NAD(P)H oxidase components gp91-phox and p22-phox in endothelial cells. *Arterioscler Thromb Vasc Biol* 2000; **20**: 1903–1911.
4. Ushio-Fukai M, Zafari AM, Fukui T, *et al*: p22phox is a critical component of the superoxide-generating NADH/NADPH oxidase system and regulates angiotensin II–induced hypertrophy in vascular smooth muscle cells. *J Biol Chem* 1996; **271**: 23317–23321.
5. Radeke HH, Cross AR, Hancock JT, *et al*: Functional expression of NADPH oxidase components (alpha- and beta-subunits of cytochrome b558 and 45-kDa flavoprotein) by intrinsic human glomerular mesangial cells. *J Biol Chem* 1991; **266**: 21025–21029.
6. Jones SA, Hancock JT, Jones OT, *et al*: The expression of NADPH oxidase components in human glomerular mesangial cells: detection of protein and mRNA for p47phox, p67phox, and p22phox. *J Am Soc Nephrol* 1995; **5**: 1483–1491.
7. Hannken T, Schroeder R, Stahl RA, Wolf G: Angiotensin II–mediated expression of p27Kip1 and induction of cellular hypertrophy in renal tubular cells depend on the generation of oxygen radicals. *Kidney Int* 1998; **54**: 1923–1933.
8. Chabrashvili T, Tojo A, Onozato ML, *et al*: Expression and cellular localization of classic NADPH oxidase subunits in the spontaneously hypertensive rat kidney. *Hypertension* 2002; **39**: 269–274.
9. Rajagopalan S, Kurz S, Munzel T, *et al*: Angiotensin II–mediated hypertension in the rat increases vascular superoxide production *via* membrane NADH/NADPH oxidase activation. Contribution to alterations of vasomotor tone. *J Clin Invest* 1996; **97**: 1916–1923.
10. Fukui T, Ishizaka N, Rajagopalan S, *et al*: p22phox mRNA expression and NADPH oxidase activity are increased in aortas from hypertensive rats. *Circ Res* 1997; **80**: 45–51.
11. Wang D, Chen Y, Chabrashvili T, *et al*: Role of oxidative stress in endothelial dysfunction and enhanced responses to angiotensin II of afferent arterioles from rabbits infused with angiotensin II. *J Am Soc Nephrol* 2003; **14**: 2783–2789.
12. Izuhara Y, Nangaku M, Inagi R, *et al*: Renoprotective properties of angiotensin receptor blockers beyond blood pressure lowering. *J Am Soc Nephrol* 2005; **16**: 3631–3641.
13. Sugiyama H, Kobayashi M, Wang DH, *et al*: Telmisartan inhibits both oxidative stress and renal fibrosis after unilateral ureteral obstruction in acatalasemic mice. *Nephrol Dial Transplant* 2005; **20**: 2670–2680.
14. Akishita M, Nagai K, Xi H, *et al*: Renin-angiotensin system modulates oxidative stress–induced endothelial cell apoptosis in rats. *Hypertension* 2005; **45**: 1188–1193.
15. Osawa E: Superaromaticity. *Kagaku* 1970; **25**: 854–863 (in Japanese).
16. Kroto HW, Heath JR, O'Brien SC, *et al*: C60: Buckminsterfullerene, *Nature* 1985; **318**: 162–163.
17. Krätschmer W, Lamb LD, Fostiropoulos K, Huffman DR: Solid C_{60}: a new form of carbon. *Nature* 1990; **347**: 354–358.
18. Krusic P, Wasserman E, Keizer P, *et al*: Radical Reactions of C60. *Science* 1991; **254**: 1183–1185.
19. Chiang LY, Upasani RB, Swirczewski JW: Versatile nitronium chemistry for C60 fullerene functionalization. *J Am Chem Soc* 1992; **114**: 10154–10157.
20. Friedman SH, DeCamp DL, Sijbesma RP, Srdanov G, Wudl F, Kenyon GL: Inhibition of the HIV-1 protease by fullerene derivatives: model building studies and experimental verification. *J Am Chem Soc* 1993; **115**: 6506–6509.
21. Tokuyama H, Yamago S, Nakamura E, *et al*: Photo-induced biochemical activity of fullerene carboxylic acid. *J Am Chem Soc* 1993; **115**: 7918–7919.
22. Krasnovsky AAJ, Foote CS: Time-resolved measurements of singlet oxygen dimol–sensitized luminescence. *J Am Chem Soc* 1993; **115**: 6013–6016.
23. Nagano T, Tanaka T, Mizuki H, Hirobe M: Toxicity of singlet oxygen generated thermolytically in *Escherichia coli*. *Chem Pharm Bull (Tokyo)* 1994; **42**: 883–887.
24. Satoh M, Matsuo K, Kiriya H, *et al*: Inhibitory effects of a fullerene derivative, dimalonic acid C60, on nitric oxide–induced relaxation of rabbit aorta. *Eur J Pharmacol* 1997; **327**: 175–181.
25. Tsuchiya T, Oguri I, Yamakoshi YN, Miyata N: Novel harmful effects of [60]fullerene on mouse embryos *in vitro* and *in vivo*. *FEBS Lett* 1996; **393**: 139–145.
26. Wang IC, Tai LA, Lee DD, *et al*: C_{60} and water-soluble fullerene derivatives as antioxidants against radical-initiated lipid peroxidation. *J Med Chem* 1999; **42**: 4614–4620.
27. Chien CT, Lee PH, Chen CF, *et al*: *De novo* demonstration and co-localization of free-radical production and apoptosis formation in rat kidney subjected to ischemia/reperfusion. *J Am Soc Nephrol* 2001; **12**: 973–982.
28. Dugan LL, Turetsky DM, Du C, *et al*: Carboxyfullerenes as neuroprotective agents. *Proc Natl Acad Sci U S A* 1997; **94**: 9434–9439.
29. Yao L, Kobori H, Rahman M, *et al*: Olmesartan improves endothelin-induced hypertension and oxidative stress in rats. *Hypertens Res* 2004; **27**: 493–500.
30. Setsukinai K, Urano Y, Kakinuma K, *et al*: Development of novel fluorescence probes that can reliably detect reactive oxygen species and distinguish specific species. *J Biol Chem* 2003; **278**: 3170–3175.
31. Burger C, Hao J, Ying Q, *et al*: Multilayer vesicles and vesicle clusters formed by the fullerene-based surfactant C60(CH3)5K. *J Colloid Interface Sci* 2004; **275**: 632–641.
32. Zhou S, Burger C, Chu B, *et al*: Spherical bilayer vesicles of fullerene-based surfactants in water: a laser light scattering study. *Science* 2001; **291**: 1944–1947.
33. O'Brien J, Wilson I, Orton T, Pognan F: Investigation of the Alamar Blue (resazurin) fluorescent dye for the assessment of mammalian cell cytotoxicity. *Eur J Biochem* 2000; **267**:

5421–5426.

34. Zalata AA, Lammertijn N, Christophe A, Comhaire FH: The correlates and alleged biochemical background of the resazurin reduction test in semen. *Int J Androl* 1998; **21**: 289–294.
35. Matsumoto K, Yamada Y, Takahashi M, *et al*: Fluorometric determination of carnitine in serum with immobilized carnitine dehydrogenase and diaphorase. *Clin Chem* 1990; **36**: 2072–2076.
36. Mizuno M, Sada T, Ikeda M, *et al*: Pharmacology of CS-866, a novel nonpeptide angiotensin II receptor antagonist. *Eur J Pharmacol* 1995; **285**: 181–188.
37. Fujiyama S, Matsubara H, Nozawa Y, *et al*: Angiotensin AT_1 and AT_2 receptors differentially regulate angiopoietin-2 and vascular endothelial growth factor expression and angiogenesis by modulating heparin binding-epidermal growth factor (EGF)–mediated EGF receptor transactivation. *Circ Res* 2001; **88**: 22–29.
38. Iwasaki Y, Ichikawa Y, Igarashi O, *et al*: Trophic effect of olmesartan, a novel AT1R antagonist, on spinal motor neurons *in vitro* and *in vivo*. *Neurol Res* 2002; **24**: 468–472.
39. Ischiropoulos H, Gow A, Thom SR, *et al*: Detection of reactive nitrogen species using 2,7-dichlorodihydrofluorescein and dihydrorhodamine 123. *Methods Enzymol* 1999; **301**: 367–373.
40. Kato Y, Mori Y, Makino Y, *et al*: Formation of N^{ε}-(hexanonyl)lysine in protein exposed to lipid hydroperoxide. A plausible marker for lipid hydroperoxide–derived protein modification. *J Biol Chem* 1999; **274**: 20406–20414.
41. Lai HS, Chen WJ, Chiang LY: Free radical scavenging activity of fullerenol on the ischemia-reperfusion intestine in dogs. *World J Surg* 2000; **24**: 450–454.
42. Lin AM, Chyi BY, Wang SD, *et al*: Carboxyfullerene prevents iron-induced oxidative stress in rat brain. *J Neurochem* 1999; **72**: 1634–1640.
43. Lee YT, Chiang LY, Chen WJ, Hsu HC: Water-soluble Hexasulfobutyl[60]fullerene inhibit low-density lipoprotein oxidation in aqueous and lipophilic phases. *Proc Soc Exp Biol Med* 2000; **224**: 69–75.
44. Sera N, Tokiwa H, Miyata N: Mutagenicity of the fullerene C60-generated singlet oxygen dependent formation of lipid peroxides. *Carcinogenesis* 1996; **17**: 2163–2169.
45. Oberdörster E: Manufactured nanomaterials (fullerenes, C60) induce oxidative stress in the brain of juvenile largemouth bass. *Environ Health Perspect* 2004; **112**: 1058–1062.
46. Isobe H, Tanaka T, Maeda R, *et al*: Preparation, purification, characterization, and cytotoxicity assessment of water-soluble, transition-metal–free carbon nanotube aggregates. *Angew Chem Int Ed Engl* 2006; **45**: 6676–6680.
47. Chiang LY, Lu F-J, Lin J-T: Free radical scavenging activity of water-soluble fullerenols. *J Chem Soc Chem Commun* 1995; **12**: 1283–1284.
48. Terao J: Antioxidant activity of beta-carotene–related carotenoids in solution. *Lipids* 1989; **24**: 659–661.
49. Olson JA: Biological actions of carotenoids. *J Nutr* 1989; **119**: 94–95.
50. Krinsky NI: Antioxidant functions of carotenoids. *Free Radic Biol Med* 1989; **7**: 617–635.
51. Korkina LG, Afanas'ev IB: Antioxidant and chelating properties of flavonoids. *Adv Pharmacol* 1997; **38**: 151–163.
52. Emmert DH, Kirchner JT: The role of vitamin E in the prevention of heart disease. *Arch Fam Med* 1999; **8**: 537–542.
53. Sun T, Xu Z: Radical scavenging activities of alpha-alanine C60 adduct. *Bioorg Med Chem Lett* 2006; **16**: 3731–3734.
54. Kawanishi S, Oikawa S, Murata M: Evaluation for safety of antioxidant chemopreventive agents. *Antioxid Redox Signal* 2005; **7**: 1728–1739.